University of California

Los Angeles

Multiple-Input Multiple-Output Orthogonal Frequency Division Multiplexing in Fast Fading Channels

A dissertation submitted in partial satisfaction

of the requirements for the degree

Doctor of Philosophy in Electrical Engineering

by

Sungsoo Kim

2003

The dissertation of Sungsoo Kim is approved.

Mario Gerla

Michael P. Fitz

Kung Yao

Gregory J. Pottie, Committee Chair

University of California, Los Angeles

2003

To my parents,

my wife, Youngsun,

and my children, Peter and Hannah

Table of Contents

List of Figures

List of Tables

Acknowledgments

Foremost, I would like to express my deepest gratitude to my advisor, Gregory J. Pottie, for his enduring support, guidance, and encouragement. He has been such a wonderful advisor that it is impossible to describe the extent of my appreciation since I joined his research group. I especially appreciated his good-natured guidance and the immense care he showed me. Without his constant support, I would not have reached to this end.

I would like to thank Professor Kung Yao, Professor Michael P. Fitz, and Professor Mario Gerla for their helpful comments and suggestions while serving on my Ph.D. committee.

I also would like to thank many fellow friends I have made during my stay at UCLA. Among them are Juno Kim, Michael Choi, Hea-Jung Kim, Bongkee Bae, Jin-Yong Lee, Jin-Sung Jung, Hong Chen, Yung-Szu Tu, Robert Thrasher, Jin-Tae Kim, and Hee-Choon Lee. I am sincerely grateful for their companionship and for their academic and nonacademic assistance.

I feel this dissertation is a tangible culmination of the last twenty four years of schooling. Throughout all this time, my parents have supported me with their balanced advice and constant encouragement. I am and will always be grateful for their love. Most of all, I would like to thank my wife, Youngsun. For more than 6 years, she has been supporting our family and my study. To her I dedicate this dissertation.

Vita

1971	Born, Seoul, Korea
1995	B.S. Electronic Engineering, Sung-Kyun-Kwan University, Suwon, Korea
1997	M.S. Electronic Engineering, Pohang University of Science and Technology, Pohang, Korea
2003	Ph.D Electrical Engineering, University of California, Los Angeles, USA

Publications

S. Kim, and G. J. Pottie, "Robust OFDM in Fast Fading Channels," *IEEE 2003 Global Communications Conference,* Dec. 2003

H. Zou, H. Kim, S. Kim, R. Wesel, W. Magione-Smith, and B. Daneshrad, "Equalized GMSK, Equalized QPSK, and COFDM, a Comparative Study for High Speed Wireless Indoor Data Communications," *IEEE 1999 Vehicular Technology Conference,* May, 1999.

S. Kim, "Fractional Delay FIR Filter and Its Application," *Master Thesis,*, Pohang University of Science and Technology, Dec., 1996.

S. Kim, W. J. Song, "A Modified Farrow Structure of Continuously Variable Fractional Delay FIR Filter," *Proc. KSPC,* Sep., 1996.

Abstract of the Dissertation

Multiple-Input Multiple-Output Orthogonal Frequency Division Multiplexing in Fast Fading Channels

by

Sungsoo Kim

Doctor of Philosophy in Electrical Engineering

University of California, Los Angeles, 2003

Professor Gregory J. Pottie, Chair

The increased data rates and reliability required to support emerging multimedia applications require new communications technology. We present results regarding two techniques used in high data rate transmission – orthogonal frequency division multiplexing (OFDM) the and multiple-input multiple-output (MIMO) scheme. The aim of this dissertation is to find efficient methods of providing reliable communication links using MIMO-OFDM under fast fading scenarios. Toward this end, both equalization and channel coding techniques are investigated.

Despite many advantages of OFDM, OFDM signals are very susceptible to the time-varying channel, which breaks the orthogonality between subcarriers, resulting in interchannel interference (ICI). The ICI increases an irreducible error floor

in proportion to the normalized Doppler frequency. A New hardware efficient equalizer, the *q-tap MMSE equalizer*, is developed to reduce ICI in MIMO-OFDM signals. Using the fact that the energy of ICI is localized in adjacent subchannels, the complexity of frequency domain MMSE equalizer can be reduced significantly without much performance degradation.

New metrics applicable for both space-time convolutional code (STCs) and space-time bit-interleaved coded modulation (ST-BICM) are developed, in order to combine the channel coding schemes with the q-tap MMSE equalizer. Simulation results showed that, for both STCs and ST-BICM, new metrics and 3-tap MMSE equalizers provide 2-3 dB gains at 10^{-5} bit error rate.

CHAPTER 1

Introduction

As applications for wireless access look to make the transition from voice communication to multimedia data, such as internet data and video data, demand for high-speed wireless communications is increasing. Also, to meet quality of service (QoS) requirements in various situations, reliability become an important issue. Orthogonal frequency division multiplexing (OFDM) is a promising candidate for high-speed transmissions in a frequency selective fading environment. By converting a wideband signal into an array of properly-spaced narrowband signals for parallel transmission, each narrowband OFDM signal suffers from frequency-flat fading and, thus, needs only a single-tap equalizer to compensate for the corresponding multiplicative channel distortion.

One disadvantage of using OFDM systems is interchannel interference (ICI) in fast fading environments. In OFDM systems, the change in the channel from symbol to symbol is more significant than for a single carrier transmission system, due to its longer symbol duration. Time variations of the channel within an OFDM symbol lead to a loss of subchannel orthogonality, resulting in interchannel interference (ICI) and leading to an irreducible error floor in conventional

OFDM receivers. Chapter 2, 3 of this dissertation provide a practical solution for designing a robust OFDM system in fast fading scenarios.

Theoretical studies of communication links employing multiple transmit and receive antennas have shown great potential for providing spectrally efficient wireless transmission. This dissertation also considers OFDM systems employing multiple transmit and receive antenna, what has been called multiple-input multiple-output (MIMO) OFDM systems. One obvious advantage of MIMO multicarrier systems over MIMO single carrier systems in a frequency-selective channel is that MIMO-OFDM greatly lessens, and possibly eliminates the need for complex equalization problem, which is a big issue for MIMO single carrier system design. This advantage is however no longer valid in fast fading environments. Chapter 4, 5 suggest a practical method for designing robust MIMO-OFDM systems in fast fading scenarios.

1.1 A Road Map

Chapter 2 begins the investigation of the interchannel interference problem in OFDM with the derivation of a mathematical model in fast fading channels. In this chapter an interchannel interference expression and its properties are presented, and a hardware efficient solution to reduce ICI is suggested. Chapter 3 investigates the channel coding problem in fast fading environments, and shows how the channel coding and equalization can work together to improve the performance of OFDM systems in fast fading channels.

Chapter 4 uses the idea of Chapter 2 to design a practical MMSE equalizer for MIMO-OFDM systems in fast fading channels. Chapter 5 presents two channel coding schemes used for MIMO-OFDM, namely, space-time convolutional codes (STCs) and space-time bit-interleaved coded modulation (ST-BICM). Based on the idea of Chapter 3, design schemes employing the channel coding with MMSE equalization are presented in this chapter. Chapter 6 presents a summary and some suggestions for future research.

1.2 Contributions

The main contributions of this dissertation are a hardware-efficient MMSE equalizer design for OFDM (and MIMO-OFDM) systems, and metrics designs used for decoding the channel codes for OFDM (and MIMO-OFDM) in fast fading channels. The details of these contributions are listed below by chapter.

- Chapter 2: Introduces the new hardware-efficient q-tap MMSE equalizer for reducing interchannel interference of OFDM signals in fast fading channels. This equalizer reduces hardware complexity significantly without losing much performance.

- Chapter 3: Applies BICM coding techniques to the q-tap MMSE equalizer using new bit-metrics for decoding.

- Chapter 4: Introduces the new hardware-efficient q-tap MMSE equalizer for reducing interchannel interference of MIMO-OFDM signals in fast fading

channels.

- Chapter 5 : Applies STCs and ST-BICM coding techniques to the q-tap MMSE equalizer using new metrics for decoding.

CHAPTER 2

OFDM in Fast Fading Channels

Orthogonal frequency division multiplexing (OFDM) is generally known as an effective modulation technique in highly frequency selective channel conditions. In OFDM systems [2–5], the entire channel is divided into many narrow subchannels. Splitting the high-rate serial data stream into many low-rate parallel streams, each parallel stream modulates orthogonal subcarriers by means of the inverse fast Fourier transform (IFFT). If the bandwidth of each subcarrier is much less than the channel coherence bandwidth, a frequency flat channel model can be assumed for each subcarrier. Moreover inserting a guard interval results in an intersymbol interference (ISI) free channel assuming that the length of the guard interval is greater than the delay spread of the channel. Therefore the effect of the multipath channel on each subcarrier can be represented by a single complex multiplier, affecting the amplitude and phase of each subcarrier. Hence the equalizer at the receiver can be implemented by a set of complex multipliers, one for each subcarrier.

Despite these advantages, however, the increased symbol duration causes adverse effects in a time-varying channel. The change in the channel from symbol

to symbol is more significant than for a single carrier transmission system. Moreover, time variations of the channel within a multicarrier symbol lead to a loss of subchannel orthogonality, resulting in interchannel interference (ICI) and leading to an irreducible error floor in conventional OFDM receivers. The performance degradation due to the interchannel interference becomes significant as carrier frequency, block size, and vehicle velocity increase.

In [6], a simplified frequency domain equalization is suggested to reduce ICI. Frequency domain equalization normally requires inversion of a large matrix. The complexity of the equalizer can be reduced significantly by using the fact that the energy of the ICI is concentrated in adjacent subchannels – in other words, only a few adjacent subchannels are major interferers to a desired subchannel. Using the minimum mean-squared error (MMSE) method, it is shown that 3 or 5-tap equalizers can perform well under fast fading.

In this chapter the channel and system models for an OFDM system under time-varying channels are described, and analysis of the ICI is presented. A new design approach with the MMSE method is introduced for the frequency domain equalization, and several simulation results are shown.

2.1 System Model under a Time-Varying Channel

In this section mathematical representations of OFDM system are presented, using an efficient vector-matrix form [7]. This representation will be used throughout this thesis, and gives us a useful tool to analyze the system. The problem of

interchannel interference (ICI) existing in an OFDM system under a time-varying channel is given. Properties of ICI are discussed, and these properties will be used for designing hardware-efficient MMSE equalizers.

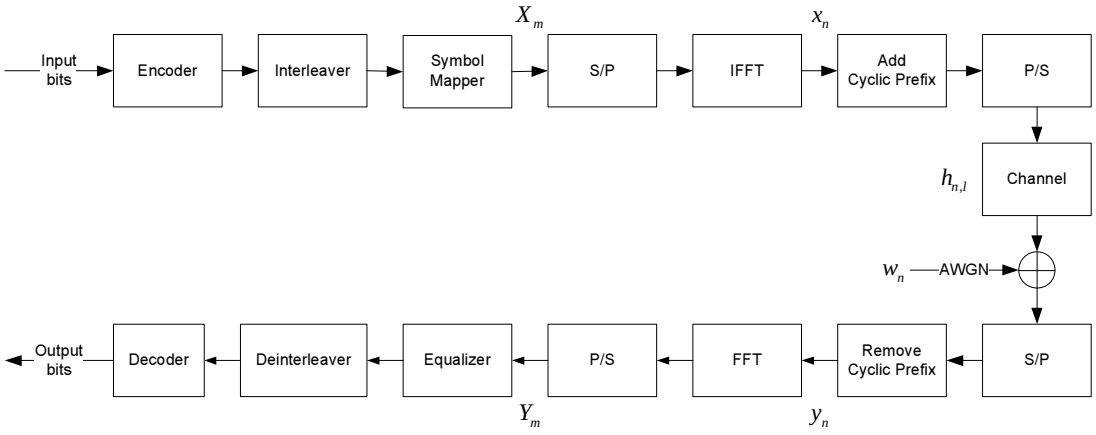

Figure 2.1: A baseband equivalent block diagram for an OFDM system

Figure 2.1 shows a discrete-time baseband equivalent model for an OFDM system. Input bits are encoded into a symbol X_m, and N symbols are sent to a serial to parallel converter (S/P). The inverse fast Fourier transform (IFFT) is then applied. The nth output of the IFFT x_n can be expressed as follows:

$$x_n = \frac{1}{\sqrt{N}} \sum_{m=0}^{N-1} X_m e^{j2\pi nm/N}, \quad n = 0, \ldots, N-1. \tag{2.1}$$

Before the parallel to serial converter (P/S), the cyclic prefix is added to avoid inter-block interference and preserve orthogonality between subchannels. Generally the length of the cyclic prefix is chosen such that the guard interval is longer than or equal to the delay spread of the channel. The cyclic prefix is ignored for simplicity in this analysis, however. By assuming that the channel consists of L multipath components, and changes at every sample, the output of the channel

can be given by

$$y_n = \sum_{l=0}^{L-1} h_{n,l} x_{n-l} + w_n, \quad n = 0, \ldots, N-1 \tag{2.2}$$

where $h_{n,l}$ and w_n represent the channel impulse response (CIR) of lth path and additive white Gaussian noise (AWGN) at time n, respectively. From (2.1), y_n can be written as

$$\begin{aligned} y_n &= \frac{1}{\sqrt{N}} \sum_{l=0}^{L-1} h_{n,l} \sum_{m=0}^{N-1} X_m e^{j2\pi(n-l)m/N} + w_n, \quad n = 0, \ldots, N-1 \\ &= \frac{1}{\sqrt{N}} \sum_{m=0}^{N-1} X_m e^{j2\pi nm/N} \sum_{l=0}^{L-1} h_{n,l} e^{-j2\pi lm/N} + w_n. \end{aligned} \tag{2.3}$$

By defining

$$H_n^{(m)} \equiv \sum_{l=0}^{L-1} h_{n,l} e^{-j2\pi lm/N}, \quad n, m = 0, \ldots, N-1 \tag{2.4}$$

where $H_n^{(m)}$ is the Fourier transform of the channel impulse response at time n. Then, y_n can be rewritten as

$$y_n = \frac{1}{\sqrt{N}} \sum_{m=0}^{N-1} X_m H_n^{(m)} e^{j2\pi nm/N} + w_n, \quad n = 0, \ldots, N-1. \tag{2.5}$$

After removing the cyclic prefix, the demodulated symbol Y_m at the receiver is obtained by applying the fast Fourier transform (FFT) so that

$$Y_m = \frac{1}{\sqrt{N}} \sum_{n=0}^{N-1} y_n e^{-j2\pi nm/N}, \quad m = 0, \ldots, N-1. \tag{2.6}$$

From (2.5), Y_m can be written as

$$\begin{aligned} Y_m &= \frac{1}{\sqrt{N}} \sum_{n=0}^{N-1} \left(\frac{1}{\sqrt{N}} \sum_{k=0}^{N-1} X_k H_n^{(k)} e^{j2\pi nk/N} + w_n \right) e^{-j2\pi nm/N}, \quad m = 0, \ldots, N-1 \\ &= \frac{1}{N} \sum_{k=0}^{N-1} X_k \sum_{n=0}^{N-1} H_n^{(k)} e^{-j2\pi(m-k)n/N} + \frac{1}{\sqrt{N}} \sum_{n=0}^{N-1} w_n e^{-j2\pi nm/N} \\ &= \left[\frac{1}{N} \sum_{n=0}^{N-1} H_n^{(m)} \right] X_m + \frac{1}{N} \sum_{k=0, k\neq m}^{N-1} X_k \sum_{n=0}^{N-1} H_n^{(k)} e^{-j2\pi(m-k)n/N} + W_m \\ &= \alpha_m X_m + \beta_m + W_m \end{aligned} \tag{2.7}$$

where

$$\alpha_m = \frac{1}{N} \sum_{n=0}^{N-1} H_n^{(m)}, \tag{2.8}$$

$$\beta_m = \frac{1}{N} \sum_{k=0, k\neq m}^{N-1} X_k \sum_{n=0}^{N-1} H_n^{(k)} e^{-j2\pi(m-k)n/N}, \tag{2.9}$$

$$W_m = \frac{1}{\sqrt{N}} \sum_{n=0}^{N-1} w_n e^{-j2\pi nm/N}. \tag{2.10}$$

Here, W_m, α_m, and β_m represent the Fourier transform of w_n, the multiplicative distortion of a desired subchannel m, and the interchannel interference caused by a time-varying channel, respectively. Note that α_m is the average frequency response of the CIR over one OFDM symbol period. If the channel is time-invariant, in other words, $H_n^{(k)}$ is not a function of n, then α_m simply becomes the frequency response of the CIR, as expected.

We can express (2.7) in a compact vector-matrix form as

$$\mathbf{y} = \mathbf{H}\mathbf{x} + \mathbf{w} \tag{2.11}$$

where $\mathbf{y} = [Y_0, \ldots, Y_{N-1}]^T$, $\mathbf{x} = [X_0, \ldots, X_{N-1}]^T$, $\mathbf{w} = [W_0, \ldots, W_{N-1}]^T$, and

$$\mathbf{H} = \begin{bmatrix} H_{0,0} & H_{0,1} & \cdots & H_{0,N-1} \\ H_{1,0} & H_{1,1} & \cdots & H_{1,N-1} \\ \vdots & \vdots & \ddots & \vdots \\ H_{N-1,0} & H_{N-1,1} & \cdots & H_{N-1,N-1} \end{bmatrix}. \tag{2.12}$$

Here, $H_{m,k}$ in (2.12) is defined as

$$H_{m,k} \equiv \frac{1}{N} \sum_{n=0}^{N-1} H_n^{(k)} e^{-j2\pi(m-k)n/N}, \quad m, k = 0, \ldots, N-1. \tag{2.13}$$

In an OFDM system over a time-varying channel, the interchannel interference can be characterized by the *normalized Doppler frequency* f_dT where f_d is the maximum Doppler frequency and T is the time duration of one OFDM symbol. Hence we can think of the normalized Doppler frequency as a maximum cycle change of the time-varying channel per OFDM symbol duration in a statistical sense.

β_m's in (2.7), or off-diagonal elements of $\mathbf{H}$ in (2.12) represent the interchannel interference (ICI) caused by the time-varying nature of the channel. In a time-invariant channel, one can easily see that β_m is zero, or $\mathbf{H}$ becomes a diagonal matrix, due to the orthogonality of the multicarrier basis waveforms. In a slowly time-varying channel, i.e., the normalized Doppler frequency f_dT is small, we can assume $E\{|\beta_m|^2\} \approx 0$. On the other hand, when the normalized Doppler frequency is high, the power of the ICI cannot be ignored, and the power of the desired signal is reduced.

2.2 Properties of ICI

According to [8], an explicit mathematical expression for ICI power can be derived. Assume that the multipath intensity profile has an exponential distribution, and the inverse Fourier transform of the Doppler spectrum is the zeroth-order Bessel function of the first kind, which is the case when the channel is in a Rayleigh fading environment. The autocorrelation function of the channel is then

$$E\left\{h_{n_1,l_1}h^*_{n_2,l_2}\right\} = c \cdot J_0\left(\frac{2\pi f_d T\left(n_1-n_2\right)}{N}\right) \cdot e^{-l_1/L}\delta\left(l_1-l_2\right) \tag{2.14}$$

where c, a normalization constant, is chosen to satisfy $c\sum_l e^{-l/L}=1$, and $J_0(\cdot)$ denotes the zeroth-order Bessel function of the first kind. Assuming the data on each subchannel are uncorrelated, and $E\{|X_m|^2\}=1$, the ICI power becomes

$$\begin{aligned} E\left\{|\beta_m|^2\right\} &= \frac{1}{N^2}\sum_{k=0,k\neq m}^{N-1} E\left\{|X_m|^2\right\} \sum_{n_1=0}^{N-1}\sum_{n_2=0}^{N-1} E\left\{H^{(k)}_{n_1}H^{(k)*}_{n_2}\right\} \cdot e^{-j2\pi(n_1-n_2)(m-k)/N} \\ &= \frac{1}{N^2}\sum_{k=0,k\neq m}^{N-1}\sum_{n_1=0}^{N-1}\sum_{n_2=0}^{N-1} E\left\{H^{(k)}_{n_1}H^{(k)*}_{n_2}\right\} \cdot e^{-j2\pi(n_1-n_2)(m-k)/N}. \end{aligned} \tag{2.15}$$

The autocorrelation of the frequency response $H^{(k)}_n$ of the channel is

$$E\left\{H^{(k)}_{n_1}H^{(k)*}_{n_2}\right\} = \sum_{l_1=0}^{L-1}\sum_{l_2=0}^{L-1} E\left\{h_{n_1,l_1}h^*_{n_2,l_2}\right\} \cdot e^{-j2\pi k(l_1-l_2)/N}. \tag{2.16}$$

From the (2.14), it becomes

$$\begin{aligned} E\left\{H^{(k)}_{n_1}H^{(k)*}_{n_2}\right\} &= \sum_{l=0}^{L-1} E\left\{h_{n_1,l_1}h^*_{n_2,l_2}\right\} \\ &= c\sum_{l=0}^{L-1} J_0\left(\frac{2\pi f_d T\left(n_1-n_2\right)}{N}\right) e^{-l/L} \\ &= J_0\left(\frac{2\pi f_d T\left(n_1-n_2\right)}{N}\right). \end{aligned} \tag{2.17}$$

Substituting (2.17) into (2.15), and using the fact that $J_0(\cdot)$ is an even function, we can simplify the ICI power expression as

$$E\left\{|\beta_m|^2\right\} = \frac{1}{N^2}\sum_{k=0,k\neq m}^{N-1}\sum_{n_1=0}^{N-1}\sum_{n_2=0}^{N-1} J_0\left(\frac{2\pi f_d T\left(n_1-n_2\right)}{N}\right)e^{-j2\pi(n_1-n_2)(m-k)/N}$$
$$= \frac{1}{N^2}\sum_{k=0,k\neq m}^{N-1}\left(N+2\sum_{n=1}^{N-1}\left(N-n\right)J_0\left(\frac{2\pi f_d T n}{N}\right)\cos\left(\frac{2\pi n\left(m-k\right)}{N}\right)\right). \tag{2.18}$$

In the same way, we can obtain

$$E\left\{|\alpha_m|^2\right\} = \frac{1}{N^2}\left(N+2\sum_{n=1}^{N-1}\left(N-n\right)J_0\left(\frac{2\pi f_d T n}{N}\right)\right). \tag{2.19}$$

Finally, we can define *total normalized ICI power* γ_m as

$$\begin{aligned}\gamma_m &\equiv \frac{E\left\{|\beta_m|^2\right\}}{E\left\{|\alpha_m|^2\right\}} \\ &= \frac{\sum_{k=0,k\neq m}^{N-1}\left(N+2\sum_{n=1}^{N-1}\left(N-n\right)J_0\left(\frac{2\pi f_d T n}{N}\right)\cos\left(\frac{2\pi n(m-k)}{N}\right)\right)}{N+2\sum_{n=1}^{N-1}\left(N-n\right)J_0\left(\frac{2\pi f_d T n}{N}\right)}.\end{aligned} \tag{2.20}$$

To obtain the distribution of ICI power among subchannels, we can define the normalized ICI power at each subchannel, $\gamma_{m,k}$. This expression can be obtained from (2.20) by simply removing the summation such that

$$\gamma_{m,k} \equiv \frac{N+2\sum_{n=1}^{N-1}\left(N-n\right)J_0\left(\frac{2\pi f_d T n}{N}\right)\cos\left(\frac{2\pi n(m-k)}{N}\right)}{N+2\sum_{n=1}^{N-1}\left(N-n\right)J_0\left(\frac{2\pi f_d T n}{N}\right)}. \tag{2.21}$$

Hence we can see

$$\gamma_m = \sum_{k=0,k\neq m}^{N-1}\gamma_{m,k}. \tag{2.22}$$

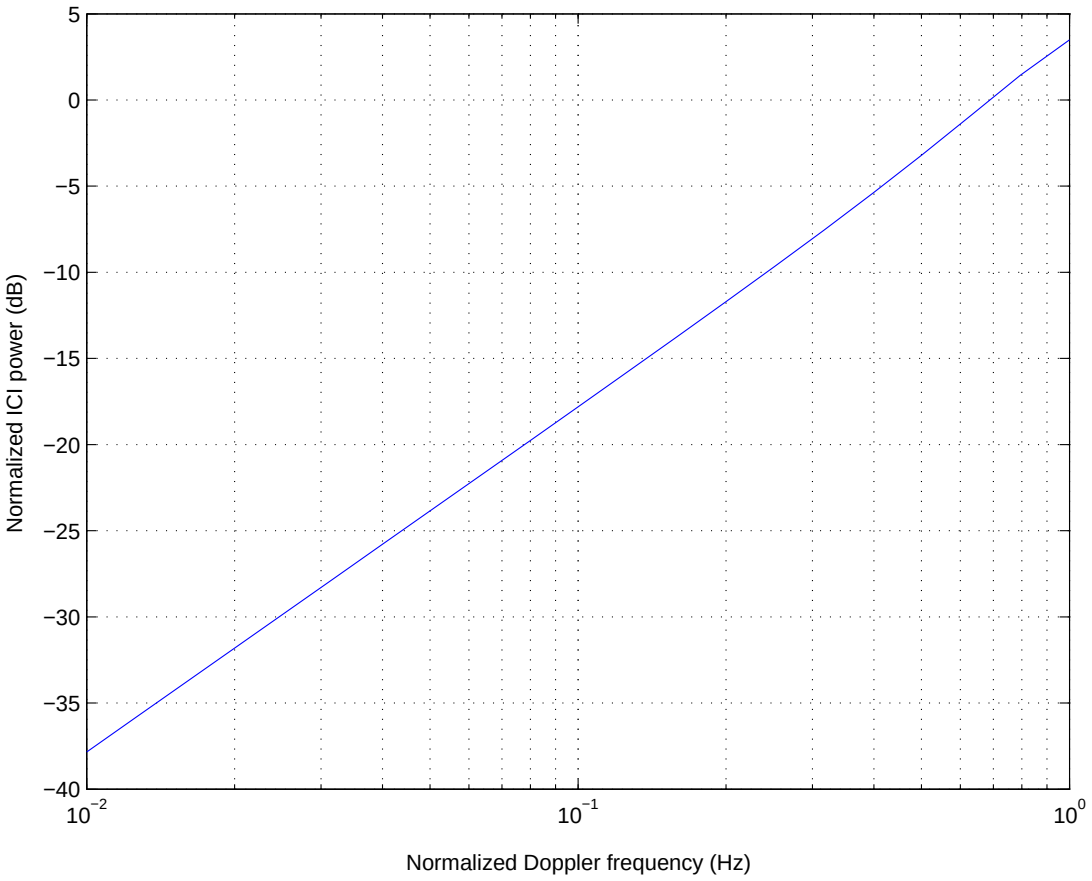

Figure 2.2: Total normalized ICI power, N=64

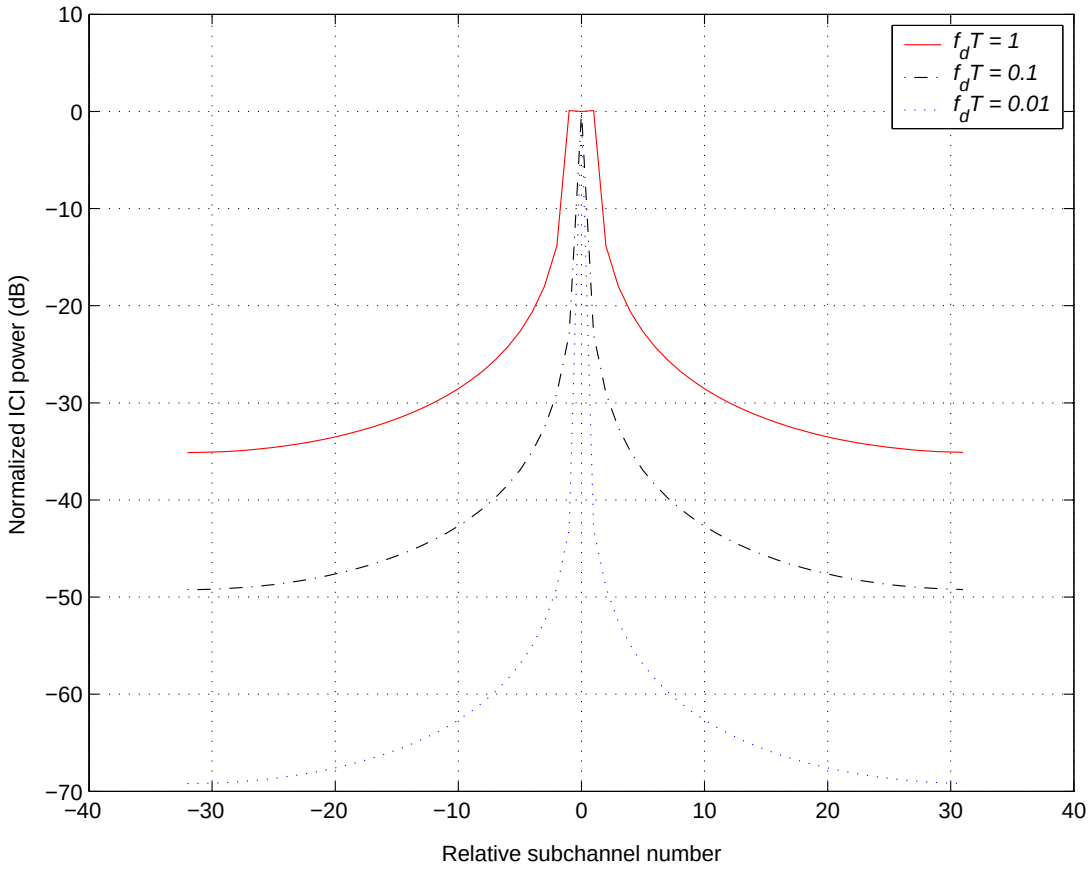

Figure 2.3: Distribution of normalized ICI power at each subchannel, N=64

Figure 2.2 illustrates the total normalized ICI power as a function of normalized Doppler frequency f_dT. As can be seen, γ_m is monotonically increasing as a function of f_dT. When $f_dT > 0.7$, the total ICI power is greater than the power of the desired signal.

Figure 2.3 shows the distribution of normalized ICI power among subchannels for different f_dT values. The overall normalized ICI power level increases as the normalized Doppler frequency increases, as expected. An important thing to see is that, as stated in [6], the ICI power tends to concentrate in the neighborhood of the desired subchannel which is set to be zero in Figure 2.3. In other words, $\gamma_{m,k_1} > \gamma_{m,k_2}$ if $|m - k_1| < |m - k_2|$ for any $0 \leq m, k_1, k_2 \leq N - 1$ and $k_1, k_2 \neq m$. Because the ICI power decreases significantly as $|m - k|$ increases, it is inefficient to use the entire set of subchannels to equalize a particular desired subchannel. This idea is the key for designing a hardware-efficient equalizer in the next chapter.

2.3 MMSE Equalizer

The conventional detection of an OFDM signal using a single tap equalizer exhibits relatively good performance at low values of f_dT. However, in an environment where the normalized Doppler frequency is high, orthogonality between subchannels breaks, and there is an irreducible error floor due to the interference induced between subchannels.

Assuming the N-by-N channel matrix $\mathbf{H}$ can be estimated, the MMSE equal-

izer can be one of the effective ways to solve this problem. The traditional way to design an MMSE equalizer in this case requires an N by N matrix inversion as well as N^2 complex multipliers, while the conventional OFDM equalizer requires only N single inversions with N complex multipliers. Since N is usually a large number, for example $N = 64$ for IEEE 802.11a, and $N \geq 2048$ for the European HDTV standard, direct implementation of the MMSE equalizer should be avoided. By exploiting the fact that the ICI power tends to be localized around a desired subchannel, complexity can be reduced significantly without losing much performance.

In this section we design MMSE equalizers using the mathematical expressions developed in the previous section. First, the traditional equalizer design approaches are adopted to obtain insight into designing MMSE equalizer in general. Then the new design method using a reduced-tap MMSE equalizer is presented. Finally, their mean-squared error performances are compared.

Consider our OFDM system model

$$\mathbf{y} = \mathbf{H}\mathbf{x} + \mathbf{w} \tag{2.23}$$

as given in (2.11). In this problem, we want to find the N-by-N equalizer matrix $\mathbf{G}$ which minimizes the cost function $E\{\|\mathbf{x} - \hat{\mathbf{x}}\|^2\}$, where $\hat{\mathbf{x}} = \mathbf{G}\mathbf{y}$ is the equalizer output vector. This is the classical MMSE design problem, and the solution is given as

$$\mathbf{G} = \mathbf{R}_{\mathbf{xy}}{\mathbf{R}_{\mathbf{y}}}^{-1} \tag{2.24}$$

where $\mathbf{R}$ denotes the covariance matrix, which is defined as $\mathbf{R}_{\mathbf{xy}} = E\left\{\mathbf{x}\mathbf{y}^{\mathrm{H}}\right\}$ and

$\mathbf{R_y} = E\left\{\mathbf{y}\mathbf{y}^{\mathrm{H}}\right\}$. Here the superscript H denotes complex conjugate transpose. The resulting MMSE is then

$$\mathrm{MMSE} = \mathrm{Tr}\left(\mathbf{R_x} - \mathbf{R_{xy}}\mathbf{R_y}^{-1}\mathbf{R_{yx}}\right) \tag{2.25}$$

where $\mathbf{R_x} = E\left\{\mathbf{x}\mathbf{x}^{\mathrm{H}}\right\}$ and $\mathbf{R_{yx}} = E\left\{\mathbf{y}\mathbf{x}^{\mathrm{H}}\right\}$, and $\mathrm{Tr}(\cdot)$ denotes the trace function. Assuming $\mathbf{H}$ is known, $\mathbf{x}$ is a zero-mean i.i.d. random vector with variance ${\sigma_x}^2$, and $\mathbf{w}$ is an AWGN vector with variance ${\sigma_w}^2$, then $\mathbf{R_{xy}}$ is

$$\begin{aligned}
\mathbf{R_{xy}} &= E\left\{\mathbf{x}\mathbf{y}^{\mathrm{H}}\right\} \\
&= E\left\{\mathbf{x}\left(\mathbf{H}\mathbf{x} + \mathbf{w}\right)^{\mathrm{H}}\right\} \\
&= \mathbf{H}^{\mathrm{H}} E\left\{\mathbf{x}\mathbf{x}^{\mathrm{H}}\right\} \\
&= \sigma_x^2 \mathbf{H}^{\mathrm{H}},
\end{aligned} \tag{2.26}$$

and $\mathbf{R_y}$ is

$$\begin{aligned}
\mathbf{R_y} &= E\left\{\mathbf{y}\mathbf{y}^{\mathrm{H}}\right\} \\
&= E\left\{\left(\mathbf{H}\mathbf{x} + \mathbf{w}\right)\left(\mathbf{H}\mathbf{x} + \mathbf{w}\right)^{\mathrm{H}}\right\} \\
&= \mathbf{H} E\left\{\mathbf{x}\mathbf{x}^{\mathrm{H}}\right\}\mathbf{H}^{\mathrm{H}} + E\left\{\mathbf{w}\mathbf{w}^{\mathrm{H}}\right\} \\
&= \sigma_x^2 \mathbf{H}\mathbf{H}^{\mathrm{H}} + \sigma_w^2 \mathbf{I}_N,
\end{aligned} \tag{2.27}$$

where $\mathbf{I}_N$ is the N-by-N identity matrix. Then (2.24) can be rewritten as

$$\mathbf{G} = \mathbf{H}^{\mathrm{H}}\left(\mathbf{H}\mathbf{H}^{\mathrm{H}} + \frac{{\sigma_w}^2}{{\sigma_x}^2}\mathbf{I}_N\right)^{-1}. \tag{2.28}$$

Likewise, (2.25) becomes

$$\mathrm{MMSE} = \sigma_x^2 \mathrm{Tr}\left(\mathbf{I}_N - \mathbf{G}\mathbf{H}\right). \tag{2.29}$$

The zero-forcing solution can be simply obtained by ignoring the noise variance from (2.28), i.e.,

$$\mathbf{G} = \mathbf{H}^{-1} \tag{2.30}$$

which is the inverse of the channel matrix $\mathbf{H}$. It is well known, however, that the zero-forcing solution experiences more noise enhancement than the MMSE approach when the channel has deep fades.

As can be seen from (2.28), the MMSE equalizer is much too complex to be implemented, especially when N is a large number. First, N-by-N matrix inversion is required to obtain the equalizer coefficient matrix $\mathbf{G}$, and N^2 complex multipliers are needed to equalize N symbols. Since the channel matrix changes in every OFDM symbol, the rate of change depends on the normalized Doppler frequency, the matrix inversion has to be performed in every N symbols as well.

2.4 q-tap MMSE Equalizer

The fact that the ICI power is localized to the neighborhood of the desired subchannel is the key for designing a new equalizer structure. Instead of using the entire set of subchannels, only a few neighborhood subchannels can be used for equalization without much performance penalty. This is true because these neighborhood subchannels contain most of the energy of the desired signal. Figure 2.4 shows the structure of the 3-tap equalizer. Only two neighborhood subchannels (one on each side) are used in this case. In this example, input symbols 1, 2, and 3 are used for equalization for the subchannel 2, and the input symbols 4, 1, 2 are

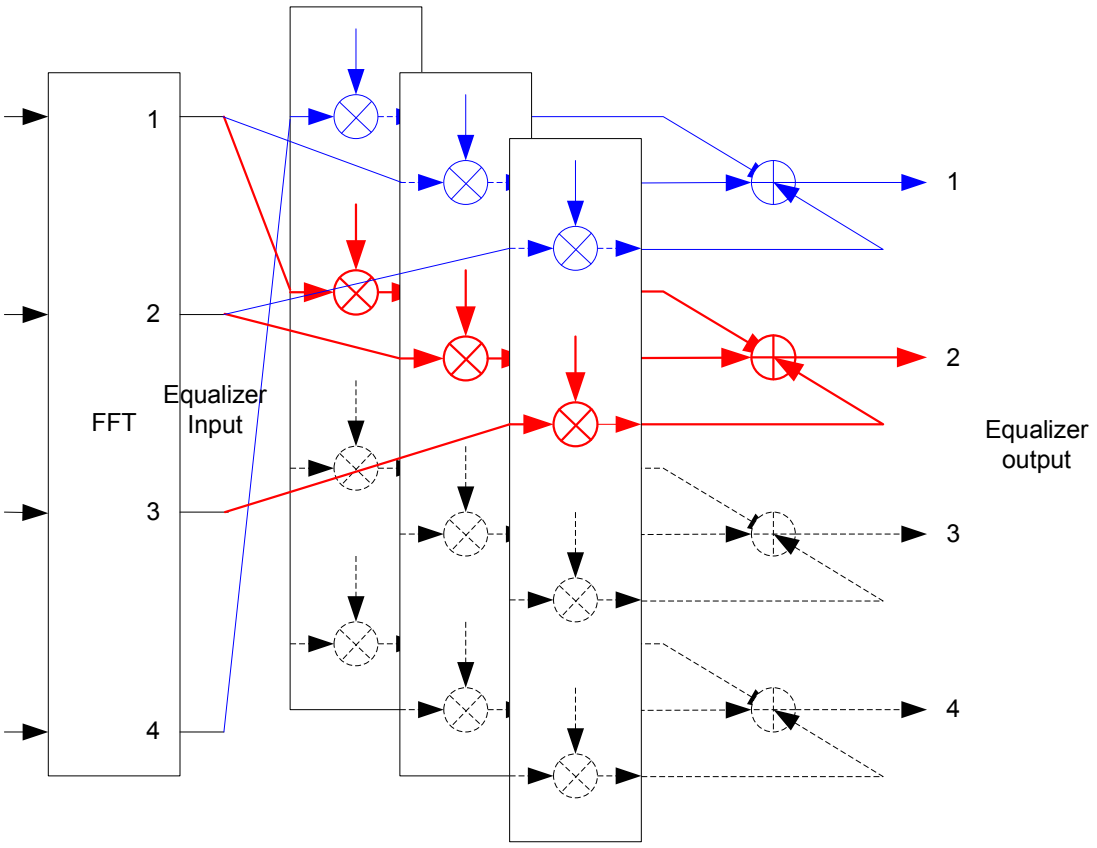

Figure 2.4: 3-tap equalizer structure

used for the subchannel 1. The example of the equalization for the subchannel2 shows that equalization for the subchannel in one edge ($m = 0$ or $m = N - 1$) requires the symbol at the other edge as well, since the channel matrix $\mathbf{H}$ is a circulant matrix in nature.

Derivation of the q-tap MMSE equalizer is similar to the MMSE case in the previous section. This time, however, we find the solution for each desired subchannel symbol individually. The problem is to find the equalizer coefficient

vector

$$\mathbf{g}_m^{(q)} = [g_{m,0}, \ldots, g_{m,q-1}] \tag{2.31}$$

which minimizes the mean-squared error

$$E\left\{\left|X_m - \hat{X}_m\right|^2\right\} \tag{2.32}$$

where $\hat{X}_m = \mathbf{g}_m^{(q)}\mathbf{y}_m^{(q)}$ and

$$\mathbf{y}_m^{(q)} = \left[Y_{(m-(q-1)/2)_N}, \ldots, Y_m, \ldots, Y_{(m+(q-1)/2)_N}\right]^{\mathrm{T}}. \tag{2.33}$$

Here $(\cdot)_N$ denotes modular function with modulus N. $\mathbf{y}_m^{(q)}$ is then

$$\mathbf{y}_m^{(q)} = \mathbf{H}_m^{(q)}\mathbf{x} + \mathbf{w}_m^{(q)} \tag{2.34}$$

where

$$\mathbf{H}_m^{(q)} = \begin{bmatrix} H_{(m-(q-1)/2)_N,0} & H_{(m-(q-1)/2)_N,1} & \cdots & H_{(m-(q-1)/2)_N,N-1} \\ \vdots & \vdots & \vdots & \vdots \\ H_{m,0} & H_{m,1} & \cdots & H_{m,N-1} \\ \vdots & \vdots & \vdots & \vdots \\ H_{(m+(q-1)/2)_N,0} & H_{(m+(q-1)/2)_N,1} & \cdots & H_{(m+(q-1)/2)_N,N-1} \end{bmatrix}, \tag{2.35}$$

and

$$\mathbf{w}_m^{(q)} = \left[W_{(m-(q-1)/2)_N}, \ldots, W_m, \ldots, W_{(m+(q-1)/2)_N}\right]^{\mathrm{T}}. \tag{2.36}$$

From (2.24), the MMSE solution is

$$\mathbf{g}_m^{(q)} = \mathbf{R}_{X_m\mathbf{y}_m^{(q)}}\mathbf{R}_{\mathbf{y}_m^{(q)}}^{-1}, \tag{2.37}$$

and, by the same assumption in the previous section, we have

$$\begin{aligned}
\mathbf{R}_{X_m \mathbf{y}_m^{(q)}} &= E\left\{ X_m \left(\mathbf{y}_m^{(q)}\right)^{\mathrm{H}} \right\} \\
&= E\left\{ X_m \left(\mathbf{H}_m^{(q)}\mathbf{x} + \mathbf{w}_m^{(q)}\right)^{\mathrm{H}} \right\} \\
&= E\left\{ X_m \mathbf{x}^{\mathrm{H}} \right\} \left(\mathbf{H}_m^{(q)}\right)^{\mathrm{H}} \\
&= \sigma_x^2 \left(\mathbf{h}_m^{(q)}\right)^{\mathrm{H}} \qquad (2.38)
\end{aligned}$$

where $\mathbf{h}_m^{(q)}$ is the mth column of the matrix $\mathbf{H}_m^{(q)}$, i.e.,

$$\mathbf{h}_m^{(q)} = \left[H_{(m-(q-1)/2)_N, m}, \ldots, H_{m,m}, \ldots, H_{(m+(q-1)/2)_N, m} \right]^{\mathrm{T}}. \qquad (2.39)$$

Also we have

$$\begin{aligned}
\mathbf{R}_{\mathbf{y}_m^{(q)}} &= E\left\{ \mathbf{y}_m^{(q)} \left(\mathbf{y}_m^{(q)}\right)^{\mathrm{H}} \right\} \\
&= E\left\{ \left(\mathbf{H}_m^{(q)}\mathbf{x} + \mathbf{w}_m^{(q)}\right) \left(\mathbf{H}_m^{(q)}\mathbf{x} + \mathbf{w}_m^{(q)}\right)^{\mathrm{H}} \right\} \\
&= \mathbf{H}_m^{(q)} E\left\{ \mathbf{x}\mathbf{x}^{\mathrm{H}} \right\} \left(\mathbf{H}_m^{(q)}\right)^{\mathrm{H}} + E\left\{ \mathbf{w}_m^{(q)} \left(\mathbf{w}_m^{(q)}\right)^{\mathrm{H}} \right\} \\
&= \sigma_x^2 \mathbf{H}_m^{(q)} \left(\mathbf{H}_m^{(q)}\right)^{\mathrm{H}} + \sigma_w^2 \mathbf{I}_q. \qquad (2.40)
\end{aligned}$$

After inserting (2.38) and (2.40) into (2.37), the q-tap equalizer vector $\mathbf{g}_m^{(q)}$ becomes

$$\mathbf{g}_m^{(q)} = \left(\mathbf{h}_m^{(q)}\right)^{\mathrm{H}} \left(\mathbf{H}_m^{(q)} \left(\mathbf{H}_m^{(q)}\right)^{\mathrm{H}} + \frac{\sigma_w^2}{\sigma_x^2} \mathbf{I}_q \right)^{-1}. \qquad (2.41)$$

In the same way, we have

$$\mathrm{MMSE} = \sigma_x^2 \sum_{m=0}^{N-1} \left(1 - \mathbf{g}_m^{(q)} \mathbf{h}_m^{(q)}\right). \qquad (2.42)$$

If we choose q as small as possible, but without sacrificing much performance, we can significantly reduce hardware complexity. For example, when $N = 64$, the

full-tap MMSE requires 64-by-64 matrix inversion with 4096 complex multipliers, while 3-tap MMSE equalizer needs 64 3-by-3 matrix inversions with only 192 complex multipliers.

2.5 Simulation Results

Figure 2.5, 2.6 illustrate the mean-squared error performance of the MMSE equalizers as a function of SNR when $f_dT = 0.01$, 0.1, 0.4, 1.0. In this simulation, the number of subchannels N is 64, and 1-tap, 3-tap, 5-tap, and full 64-tap MMSE equalizers are under consideration. Figure 2.5(a) shows that different numbers of taps do not make any difference at a low f_dT. This means, at a low f_dT, only the equalizer coefficient of the desired subchannel has a non-zero value, since the ICI power is almost zero. When $f_dT = 0.1$ in Figure 2.5(b), the performance difference becomes larger, especially when SNR is high. Note that the curve for the full MMSE equalizer is almost a straight line, which means the full MMSE equalizer does not have an irreducible error floor due to the ICI, unlike the other cases. The problem with the irreducible error floor becomes more distinct for the 1-tap equalizer when $f_dT = 0.4$ in Figure 2.6(a) and $f_dT = 1.0$ in Figure 2.6(b). Also note that the error floor decreases as the number of equalizer taps increases. In Figure 2.6(b), the gain from the multiple-tap equalizers over the single-tap approach is much larger even in very low SNR region such as 0 dB $\leq$ SNR $\leq$ 5 dB. This is because the ICI dominates the overall interference-noise level over the background noise.

Figure 2.7, 2.8 show the MSE performance as a function of f_dT when SNR is 0, 10, 20, and 30 dB. Generally more gain can be achieved with multiple-tap equalizers as SNR increases. When SNR is 20 dB in Figure 2.8(a), the 3-tap equalizer has about 2 dB gain compared to the 1-tap equalizer but 2 dB loss compared to 64 taps. Also, when SNR is 30 dB in Figure 2.8(b), the 5-tap equalizer has about 6 dB gain compared to one tap, but 5 dB loss compared to the full-tap MMSE equalizer.

2.6 Summary

This chapter began with the derivation of a mathematical model for OFDM systems in fast fading channels. An interchannel interference expression was presented from the system model. It was shown that the energy of ICI is localized in a desired subchannel.

As a solution to reduce ICI, frequency domain MMSE equalizer was suggested. It was demonstrated that conventional MMSE approach is not feasible, due to the large number N. Also it was shown that, using the ICI property, the complexity of MMSE equalizer can be reduced considerably with a small MSE performance loss.

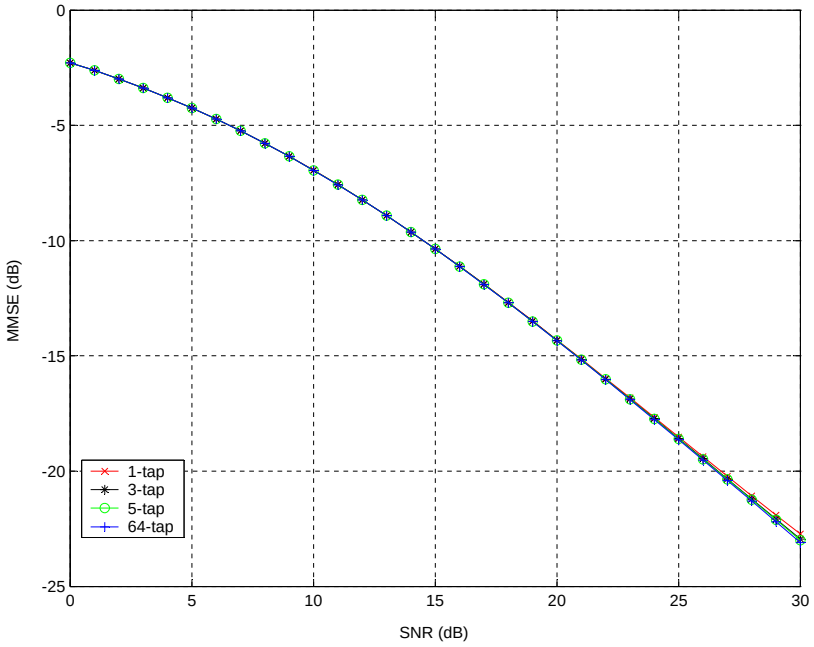

(a) $f_dT = 0.01$

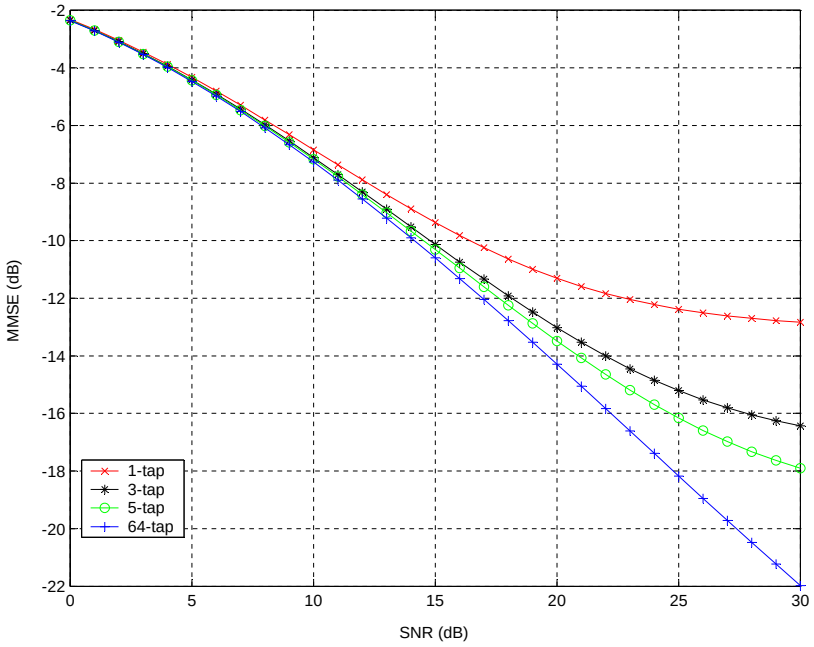

(b) $f_dT = 0.1$

Figure 2.5: MSE performance of MMSE equalizers for $f_dT = 0.01, 0.1$

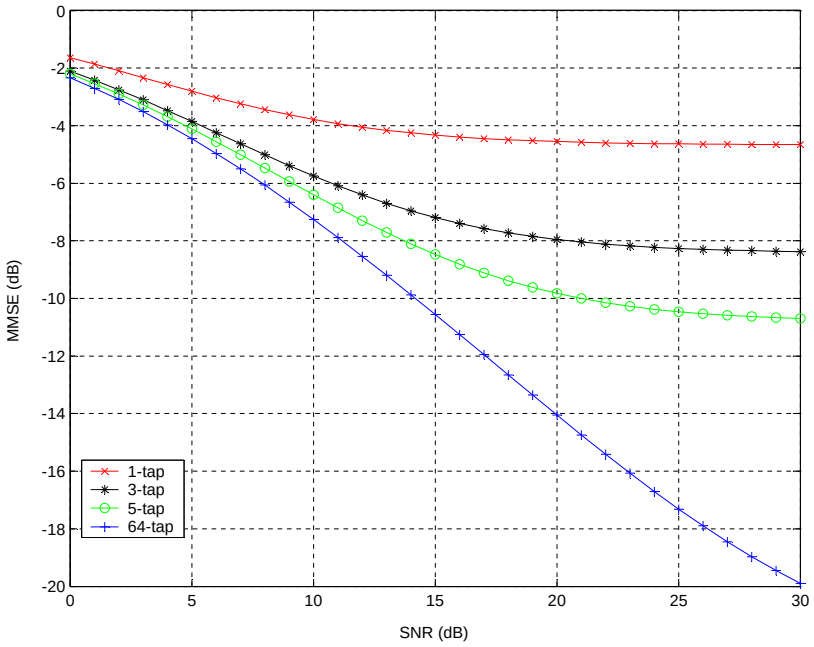

(a) $f_dT = 0.4$

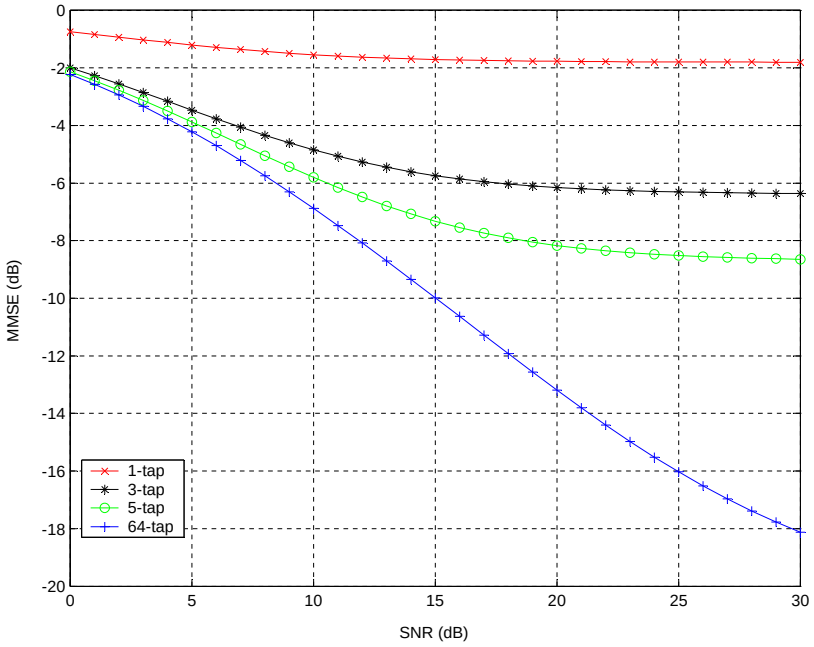

(b) $f_dT = 1.0$

Figure 2.6: MSE performance of MMSE equalizers for $f_dT = 0.4, 1.0$

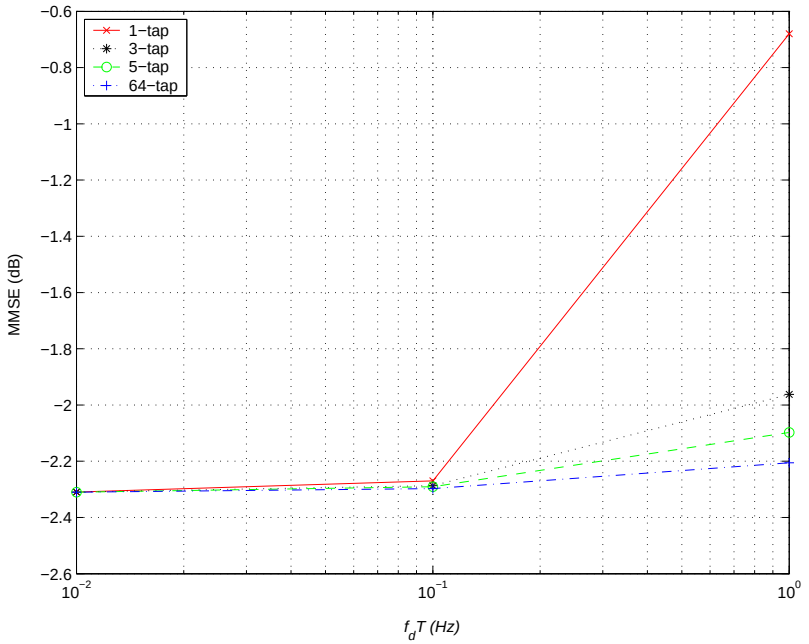

(a) SNR = 0 dB

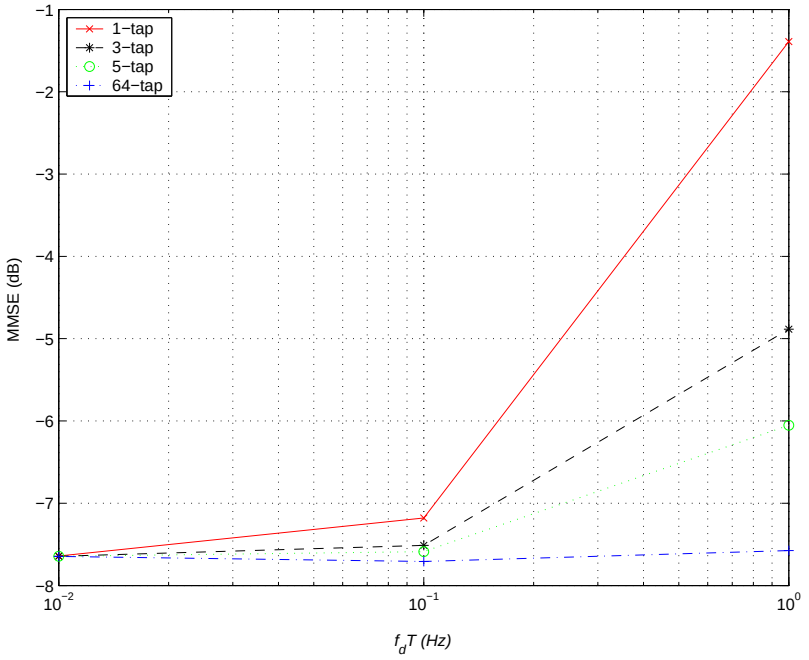

(b) SNR = 10 dB

Figure 2.7: MSE performance of MMSE equalizers for SNR = 0, 10 dB

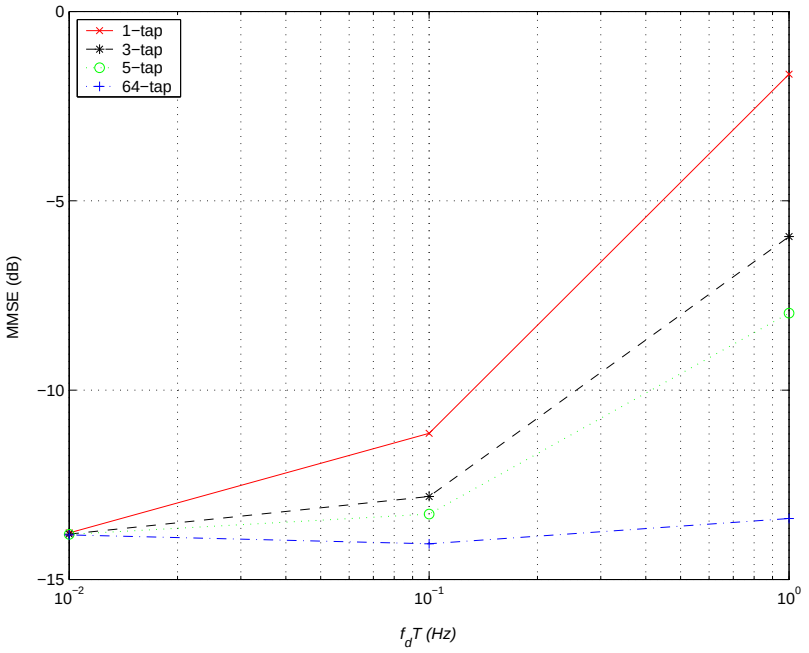

(a) SNR = 20 dB

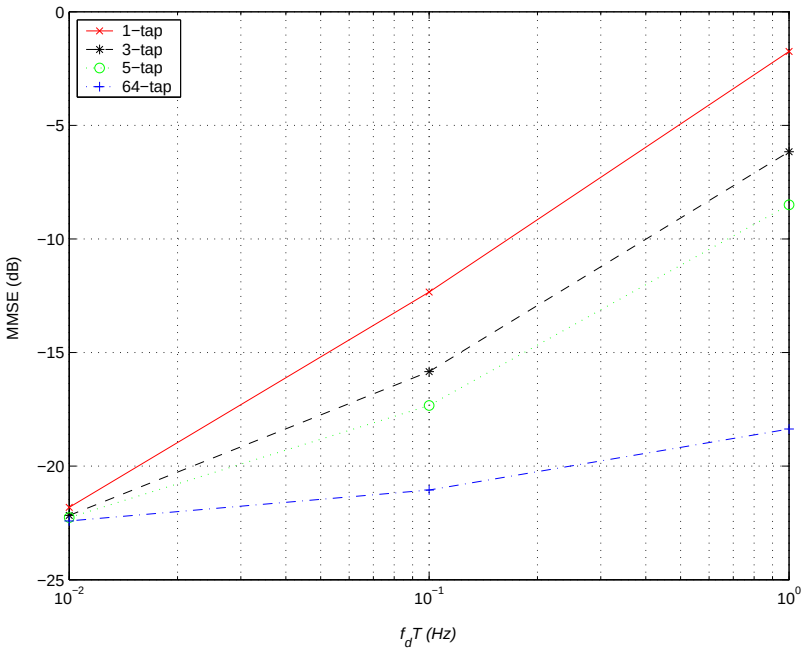

(b) SNR = 30 dB

Figure 2.8: MSE performance of MMSE equalizers for SNR = 20, 30 dB

CHAPTER 3

Channel Coding for OFDM in Fast Fading Channels

The reliability of digital communication over a fading channel can be much improved by means of channel coding. For example, an M-ary channel signal constellation can be used in conjunction with trellis codes [9]. The coding gain is achieved by constructing a code using expanded signal sets and a convolutional encoder. Some improvement in the sense of the coding gain can be obtained by searching for optimal codes according to some additive metric, which takes into account the combined weight of the Euclidean distance and the diversity of the code. The disadvantage of this approach is that the order of diversity remains equal to the minimum number of distinct symbols between two codewords.

The bit-interleaved coded modulation (BICM) technique, based on a convolutional code followed by $\log(M)$ bit interleavers, yields a better coding gain over a Rayleigh fading channel than the original trellis-coded modulation (TCM) [10]. The diversity of a coded system can be increased with this approach. This diversity is proportional to d_{free} of the code, and the error performance is governed by some product of d_{free} terms. Here, d_{free} is the free binary Hamming distance

of the code. At first glance it seems that there are two major problems. First, since the bit interleavers induce a random mapping it is not clear that a good convolutional code yields a good coded system. Second, what type of metric is to be used before the metric deinterleavers at the receiver side?

In this chapter, the BICM decoding method is introduced and it is shown that the error performance of the BICM system is superior to that of the existing TCM system over a Rayleigh fading channel. Also the BICM technique is applied to the OFDM with the MMSE equalizer designed in the previous chapter. Bit-error rate performance is compared under various circumstances.

3.1 BICM under a Rayleigh Fading Channel

An example of the BICM system is shown in Figure 3.1. In this example, a binary sequence $\mathbf{i}_n$ at time n is encoded into another binary sequence $\mathbf{c}_n$ using a rate $R = \frac{3}{4}$, convolutional code with a 16-QAM modulator. We shall represent the binary (0,1) input and the binary output sequences of a convolutional encoder by $\mathbf{i}_n = [i_n^1, i_n^2, i_n^3, i_n^4]$, and $\mathbf{c}_n = [c_n^1, c_n^2, c_n^3, c_n^4]$, respectively. The encoder outputs are fed into four independent ideal interleavers, resulting in a binary vector $\mathbf{c}_n{}' = \left[c_n^{1\prime}, c_n^{2\prime}, c_n^{3\prime}, c_n^{4\prime}\right]$. A group of 4 bits at the output of the interleavers is mapped into the 16-QAM signal set x_n, according to Gray mapping (Figure 3.3(b)). The mapping signal points are digitally pulse shaped, and transmitted over the channel. At the receiver, a faded noisy version of the transmitted channel

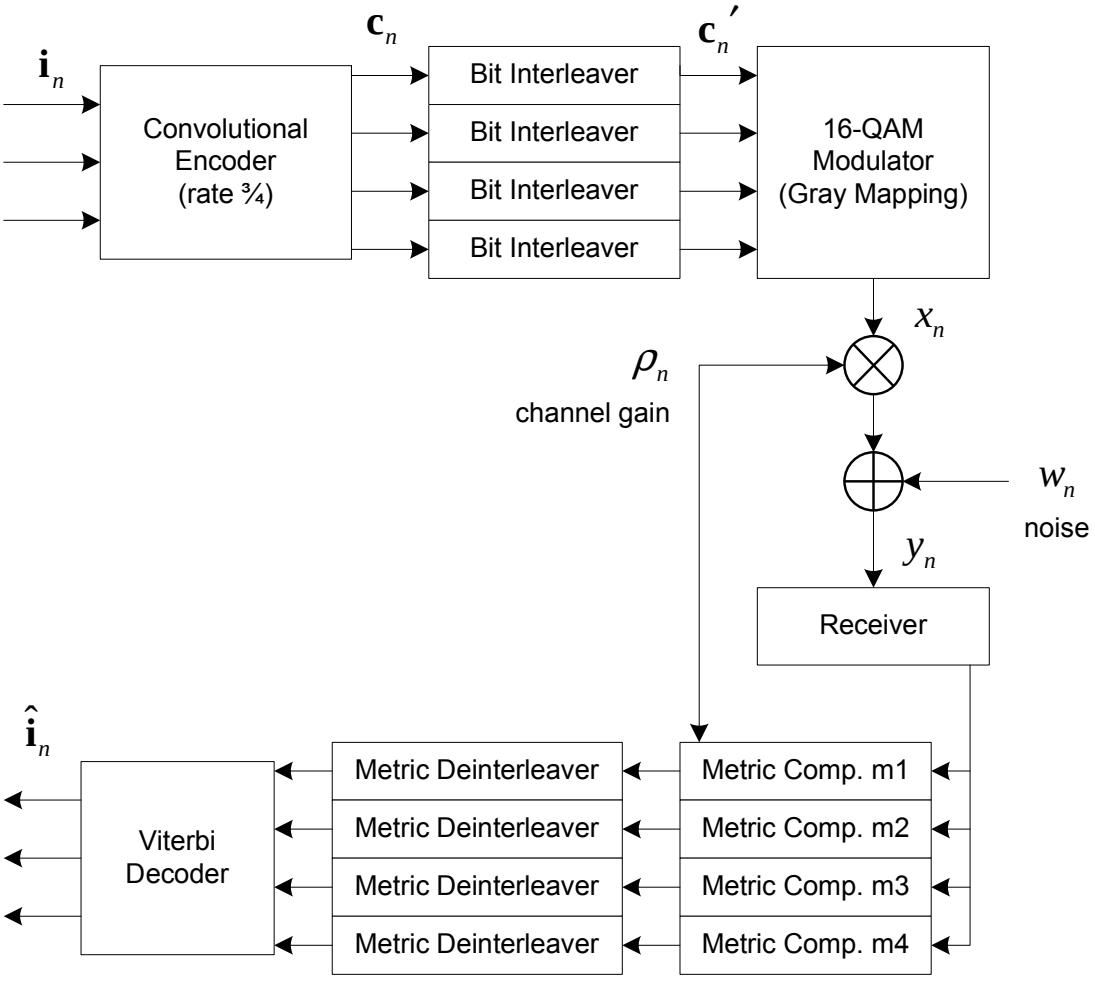

Figure 3.1: Block diagram of BICM system

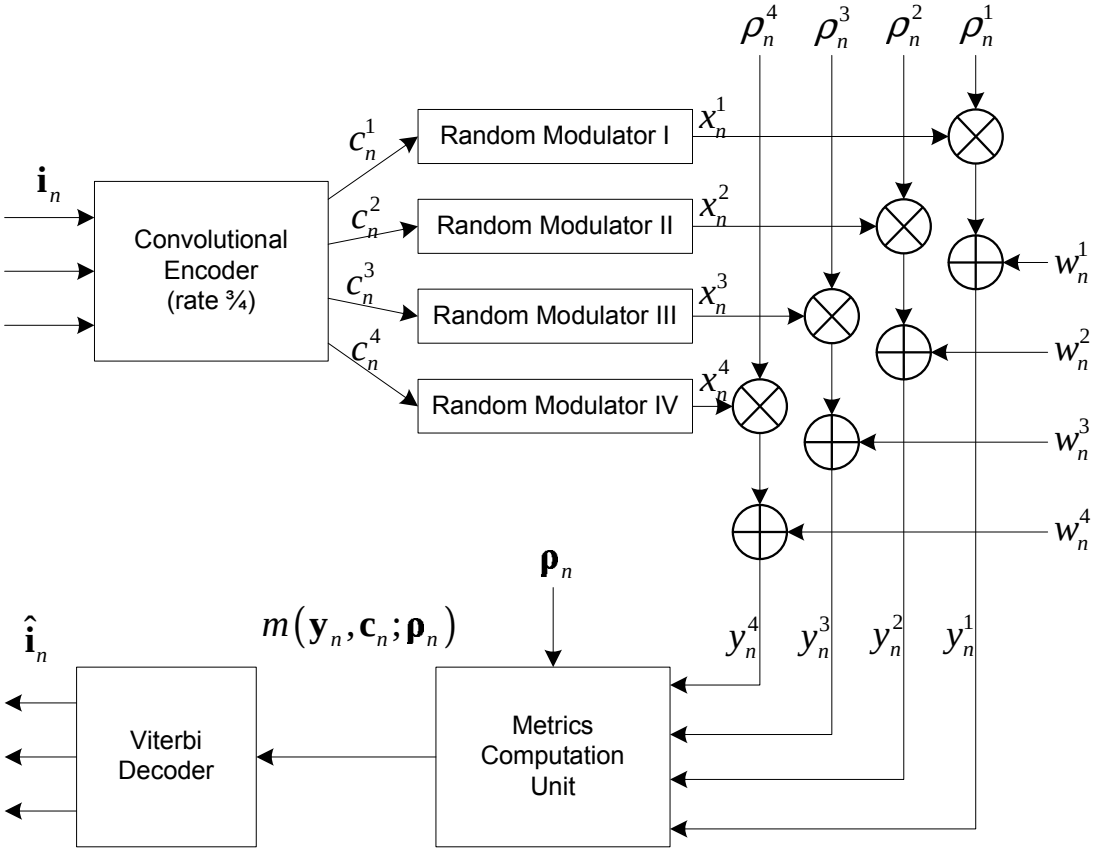

Figure 3.2: Analysis model of BICM system

signal y_n can be written as

$$y_n = \rho_n x_n + w_n \tag{3.1}$$

where ρ_n is a random variable representing the random amplitude of the received signal, and w_n is a complex zero-mean Gaussian random variable with variance ${\sigma_w}^2$. The received signal is then passed through a demodulator, four metric computation units, and metric deinterleavers. Finally, the decision on the transmitted sequence is taken with the aid of the Viterbi decoder.

An analysis model of the BICM system is shown in Figure 3.2. In what follows, ideal interleavers and deinterleavers are assumed, so that the combined interleavers and mapping can be viewed as four statistically independent communication modulators and channels. The output of the encoder $\mathbf{c}_n$ is transmitted by four random modulators. There are four transmitted symbols, x_n^i, $i = 1, 2, 3, 4$, carrying the encoder output bits c_n^i. With ideal random interleavers, any one of the eight possible transmitted symbols associated with a fixed value of c_n^i for a particular ith bit, may appear with equal probability. With the mapping from binary to 16-QAM symbols, we define the subsets, S_i^0 and S_i^1, $i = 1, 2, 3, 4$, based on whether the bit is 0 or 1 at each bit position, as shown in Figure 3.3(b). The transmitted symbols associated with an output bit $c_p^i = c$ at time n can be any symbol from the subset S_i^c $(c = 0, 1)$ with equal probability, 1/8. Thus, the ith bit c_n^i, induces a partition of the signal set into two subsets S_i^0 and S_i^1, $i = 1, 2, 3, 4$, as it is shown in Figure 3.3(b).

This model of random modulation is due to the random interleavers, and to

the suboptimal nature of the BICM system which does not use the side information associated with the ordering of the transmitted symbols.

At the receiver, the faded, noisy version of the transmitted symbol is passed through four metric computation units. An optimal decoder calls for a complicated metric which takes into account a priori probabilities of transmission of all possible eight transmitted symbols from the set S_i^0 or S_i^1 associated with the output bit c_n^i. In selecting a decoding metric, a tradeoff exists between simplicity of implementation, robustness of the system, and error performance. For the BICM system in [10], a receiver which uses the suboptimal metric

$$m_i\left(y_n^i, S_i^c; \rho_n^i\right) = \min_{x \in S_i^c} \left|y_n^i - \rho_n^i x\right|^2, \quad c = 0, 1, \quad i = 1, 2, 3, 4, \tag{3.2}$$

is suggested. Here, y_n^i is the received signal at the ith bit position at time n. Each ith metric computation unit produces two metrics corresponding to the two possible values of the bit c_n^i, at time n. The decoder input unit computes the branch metrics corresponding to all possible values of $\mathbf{c}_n = [c_n^1, c_n^2, c_n^3, c_n^4]$ – in this example the number of possible branch metrics is $2^4 = 16$. For each such value the decoder input unit computes the sum

$$m\left(\mathbf{y}_n, \mathbf{c}_n; \rho_n\right) = \sum_{i=1}^{4} \left(1 - c_n^i\right) m_i\left(y_n^i, S_i^0; \rho_n^i\right) + c_n^i m_i\left(y_n^i, S_i^1; \rho_n^i\right), \tag{3.3}$$

where $\rho_n = [\rho_n^1, \rho_n^2, \rho_n^3, \rho_n^4]$. Finally, these metrics are fed to the decoder, which employs the Viterbi algorithm to find the binary data sequence with the smallest cumulative sum of metrics, $m\left(\mathbf{y}_n, \mathbf{c}_n; \rho_n\right)$.

Bit-error rate (BER) performance of the BICM system under a Rayleigh fading channel is shown in Figure 3.4. In this simulation, an infinite-length ideal

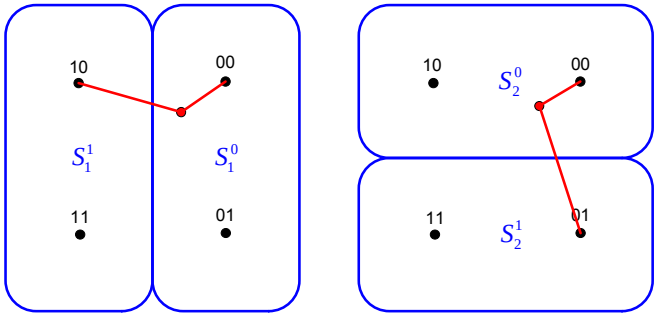

(a) 4-QAM

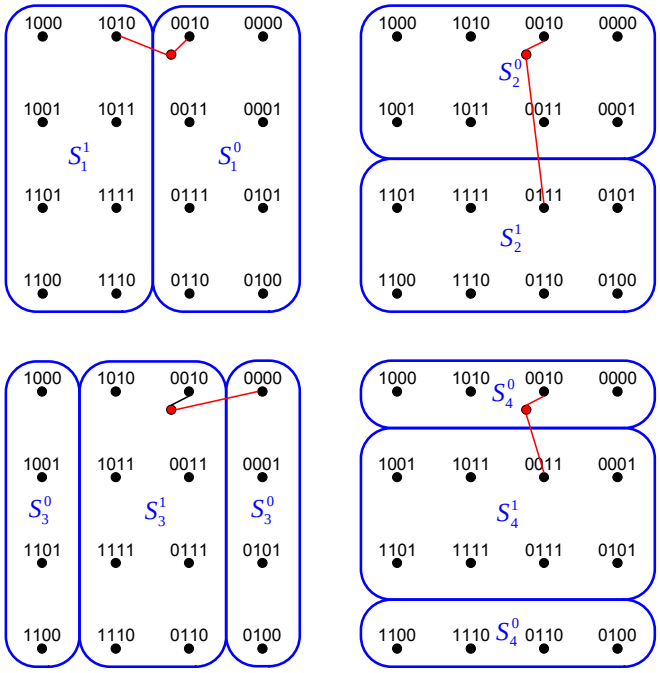

(b) 16-QAM

Figure 3.3: Partitions of signal set to subsets '0' group and '1' group

interleaver and deinterleaver is assumed, so that each combined unit of interleaver and symbol mapping becomes statistically independent. The number of bits per symbol is 2, and Figure 3.3(a) is used for the symbol mapping and signal set partitioning. The encoder is a 64-state convolutional encoder with rate 1/2. It is seen that BICM requires $E_b/N_o = 7.5$ dB for BER $= 10^{-5}$, while TCM needs $E_b/N_o = 9.0$ dB. Note that most of the coding gain was obtained through the diversity of the code, generated by the bit interleavers. This gain is larger than the loss associated with the random nature of the modulation and the suboptimal decoding. This result indicates that the error performance of BICM improves compared to conventional TCM with equal decoding complexity. Note, however, that due to the interleavers the decoding delay and the memory storage requirements are larger. BER performance for uncoded systems under a Rayleigh fading channel and an AWGN channel are also provided for reference.

3.2 BICM with q-tap MMSE Equalizer

An OFDM system is an attractive modulation technique for the system employing a convolutional code because of its inherent orthogonality. As far as there is no ICI in OFDM systems, each subchannel can be viewed as an independent flat fading channel – in other words a memoryless channel, so that the maximum-likelihood decoding process is straightforward with the Viterbi decoder. Single carrier systems under multipath channels, on the other hand, suffer from inter-symbol interference (ISI) so that a much more complex algorithm is required for

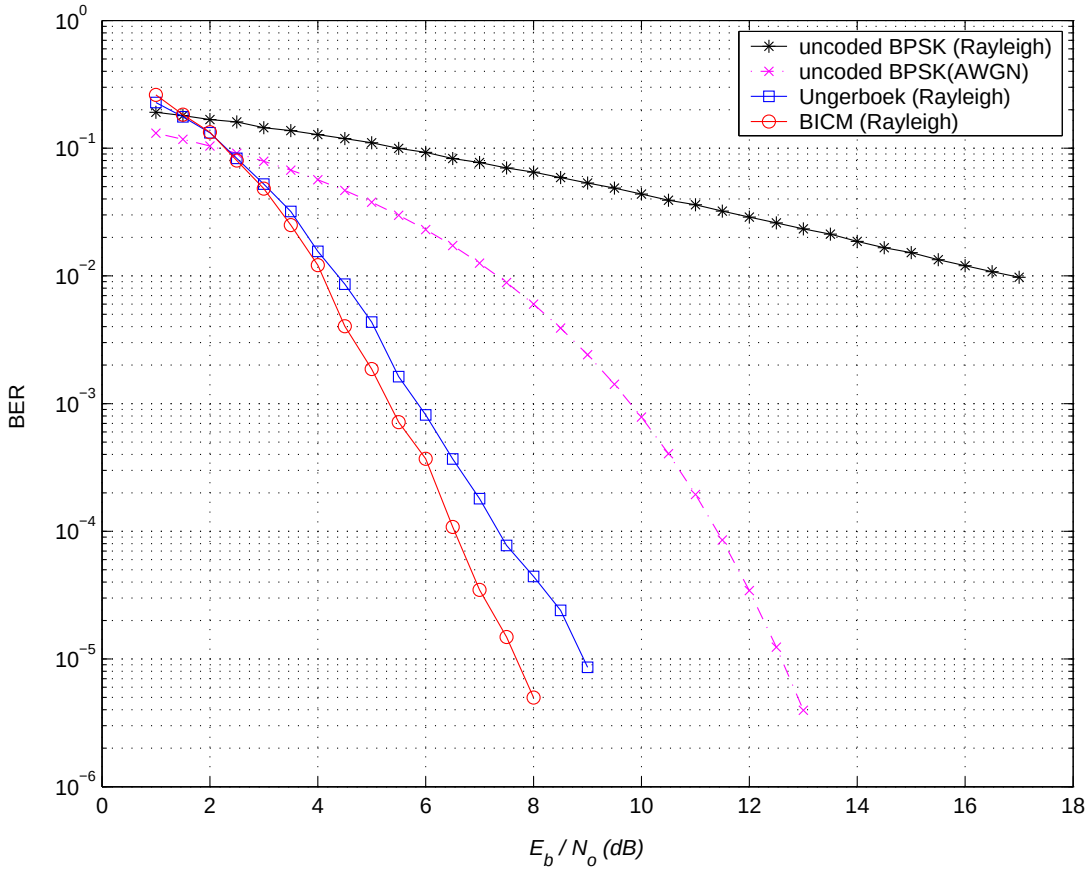

Figure 3.4: Bit-error rate performance of BICM system: 4-QAM, 64 states, rate 1/2

maximum likelihood decoding. When the normalized Doppler frequency is large, however, OFDM is also in the same situation as the single carrier system because of the ICI.

In the previous section ideal infinite-length bit interleavers are assumed, but it cannot be true in a real situation. Diversity for BICM can be maintained only when the length of the bit interleavers is long enough so that independence between bits is preserved. With fixed length bit interleavers, BICM under a fast fading channel may perform better than BICM under slow fading.

We can combine BICM and the q-tap MMSE equalizer designed in the previous chapter to increase diversity as well as signal to noise ratio. The problem with this combination is to determine what metric is appropriate in the presence of the equalizer. If we use BICM alone for the OFDM system without ICI, then the metrics should be the same as (3.3), i.e.,

$$M_0 \equiv \min_{x \in S^c} |y_m - H_{m,m}x|^2, \quad c = 0, 1 \tag{3.4}$$

where $H_{m,m}$ in (2.13) is the channel gain at the subchannel m. Note that off-diagonal elements of $\mathbf{H}$ in (2.12) are all zeros since there is no ICI. In the presence of equalizers, however, M_0 cannot be used directly since y_m is not the channel output as in (3.1), but the equalizer output $\hat{x}_m$. Hence the simplest metrics in the presence of equalizers could be

$$M_1 \equiv \min_{x \in S^c} |\hat{x}_m - x|^2, \quad c = 0, 1. \tag{3.5}$$

The M_1, however, does not include the subchannel gain information which may improve the performance greatly. If we scale the metrics based on the power of

each subchannel, then we have

$$M_2 \equiv \min_{x \in S^c} |\hat{x}_m - x|^2 \, |H_{m,m}|^2, \quad c = 0, 1. \tag{3.6}$$

We can improve further by examining the equalizer output,

$$\begin{aligned} \hat{x}_m &= \mathbf{g}_m^{(q)} \mathbf{y}_m^{(q)} \\ &= \mathbf{g}_m^{(q)} \left(\mathbf{H}_m^{(q)} \mathbf{x} + \mathbf{w}_m^{(q)} \right) \\ &= \mathbf{g}_m^{(q)} \mathbf{h}_m^{(q)} x_m + \mathbf{g}_m^{(q)} \left(\mathbf{w}_m^{(q)} + \mathbf{w}_m^{(q)'} \right) \end{aligned} \tag{3.7}$$

where $\mathbf{g}_m^{(q)} = [g_{n,0}, \ldots, g_{n,q-1}]$ is the equalizer coefficient vector, the channel matrix $\mathbf{H}_m^{(q)}$ is from (2.35), and $\mathbf{h}_m^{(q)}$ is mth column of $\mathbf{H}_m^{(q)}$. Here $\mathbf{w}_m^{(q)'}$ denotes a residual ICI term after the equalizer. Since

$$\begin{aligned} \left| \hat{x}_m - \mathbf{g}_m^{(q)} \mathbf{h}_m^{(q)} x_m \right|^2 &= \left| \mathbf{g}_m^{(q)} \left(\mathbf{w}_m^{(q)} + \mathbf{w}_m^{(q)'} \right) \right|^2 \\ &\simeq \left| \mathbf{g}_m^{(q)} \right|^2 \left| \mathbf{w}_m^{(q)} + \mathbf{w}_m^{(q)'} \right|^2, \end{aligned} \tag{3.8}$$

new metrics can be written as

$$M_3 \equiv \frac{1}{\left| \mathbf{g}_m^{(q)} \right|^2} \min_{x \in S^c} \left| \hat{x}_m - \mathbf{g}_m^{(q)} \mathbf{h}_m^{(q)} x \right|^2. \tag{3.9}$$

3.3 Simulation Results

Figure 3.5 compares BER performance for different metrics. In this simulation the number of subcarrier N=32, the normalized Doppler frequency $f_d T$=0.4, 4-QAM modulation, and 64-state convolutional code with rate 1/2 are used. As expected, the performance order is $M_1 < M_2 < M_3$. At BER=10^{-4}, M_3 has 1.2 dB gain over M_2, and 0.2 dB over M_1 for the 3-tap MMSE equalizer.

Figure 3.6, 3.7 show BER performance under various conditions. When $f_dT = 0.4$ as shown in Figure 3.7, only the systems having both coding and an equalizer do not suffer from serious ICI degradation. Note that both '1-tap with BICM' and 'BICM only' have an irreducible error floor due to the severe ICI impairments. When $f_dT = 0.1$, it seems that increasing the number of taps for the MMSE equalizer is not effective, but it is not generally true. This is because higher-tap equalizers have a small gain advantage in the low SNR region, as shown in Figure 2.5, 2.7. Even in this low SNR region, we can still notice about 0.7 dB gain for '3-tap equalizer with BICM' compared to 'BICM only' system.

3.4 Testbed Results

Hardware research project for MIMO-OFDM systems is in progress at UCLA's Wireless Integrated Systems Research Group (WISR Group). As a part of the research, a preliminary testbed has been built for initial performance testing. The testbed is mainly a PC-based system, in which most signal processing is performed by the PC, except the RF front end and antennas for over-the-air wireless transmission. The test is performed in an indoor office environment where the transmitter and the receiver are in a fixed location, and a direct line-of-site exists between the transmit and the receive antennas. The testbed uses a 512-point FFT/IFFT with QPSK symbol mapping. Since the calibration of the testbed had not been completed at the time of testing, approximately 5% error of transmitted symbols is detected. Figure 3.8 shows the original transmitted

images, which have 449 by 400 pixels with 4 level gray scale. BICM algorithm is applied to the testbed. Figure 3.9 and 3.10 demonstrate the performance of the BICM algorithm. In Figure 3.9, the error rate of the uncoded image is 4.98%, while the BICM coded error rate is 0.077%. In Figure 3.10, the uncoded image has 6.84% error, while the BICM coded error rate was only 0.032%.

3.5 Summary

This chapter introduced bit-interleaved coded modulation (BICM), which provides better performance than the traditional Ungerboeck's trellis coded modulation (TCM) approach in Rayleigh fading channels. It was shown that BICM can be used with q-tap MMSE equalizer designed in Chapter 2 in order to increase robustness of OFDM systems in fast fading scenarios. For the combination of the BICM and the q-tap MMSE equalizer, several new bit metrics were suggested. Simulation results showed that the suggested solution provides robust performance even in a very high normalized Doppler frequency, such as 0.4.

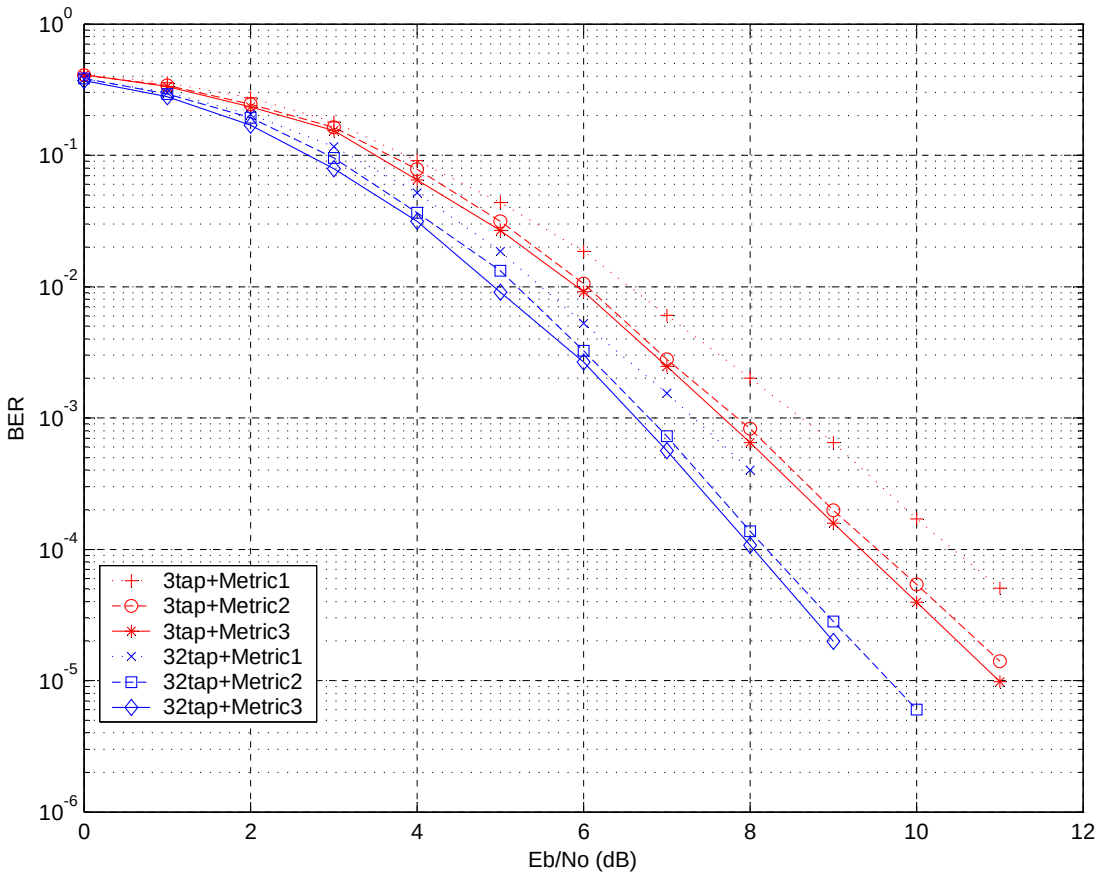

Figure 3.5: BER performance for different metrics: $N = 32$, $f_dT = 0.4$, 4-QAM, 64 states, rate 1/2

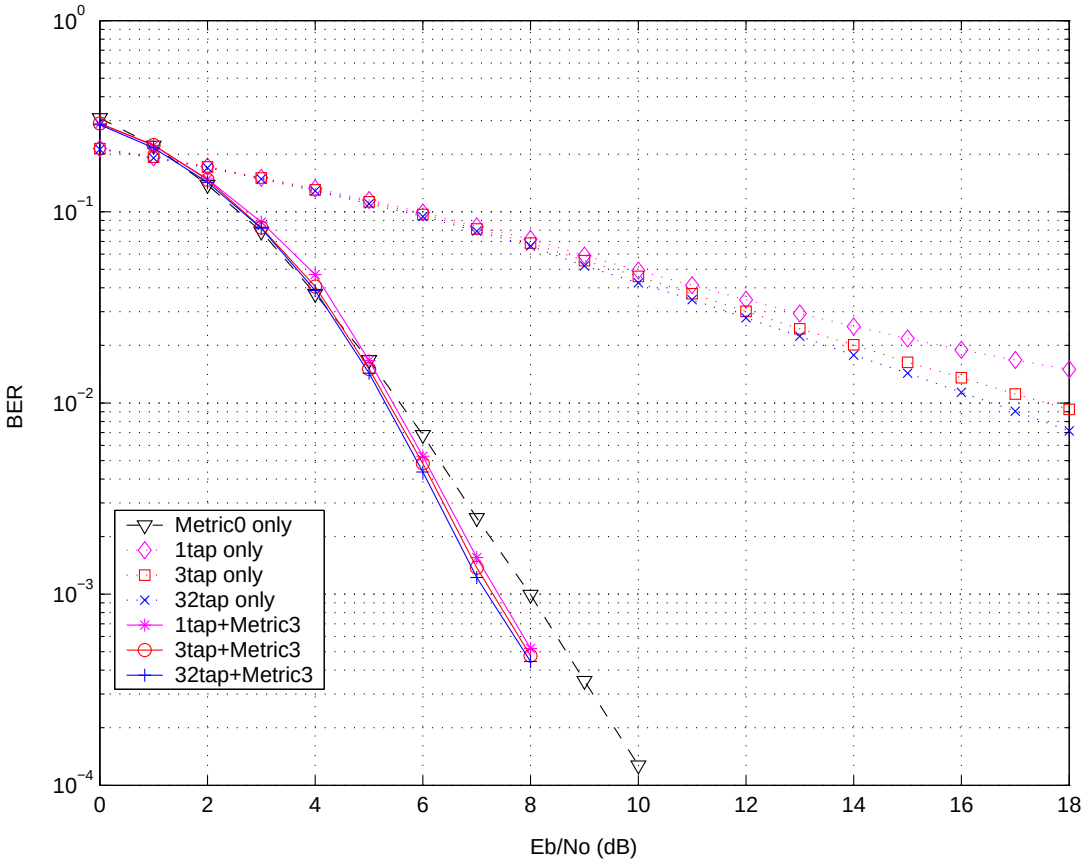

Figure 3.6: BER performance under various conditions: $f_dT = 0.1$, $N = 32$, 4-QAM, 64 states, rate 1/2

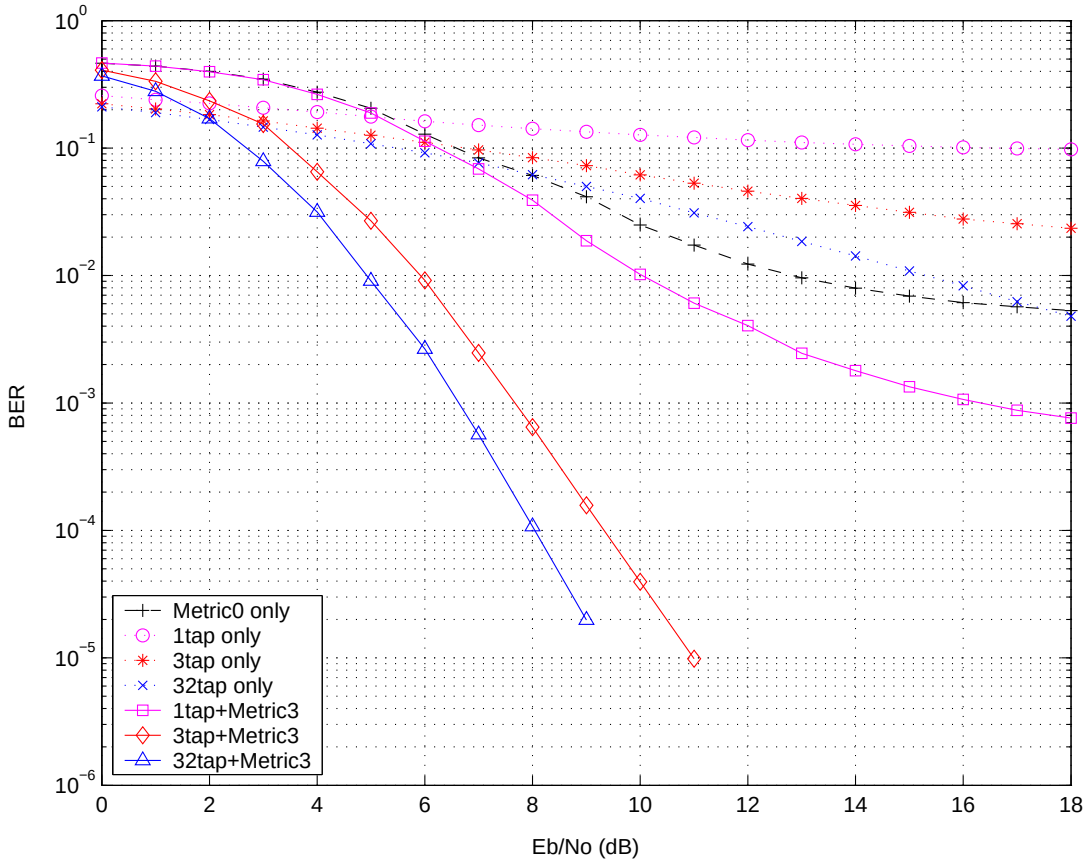

Figure 3.7: BER performance under various conditions: $f_dT = 0.4$, $N = 32$, 4-QAM, 64 states, rate 1/2

(a) Wood image

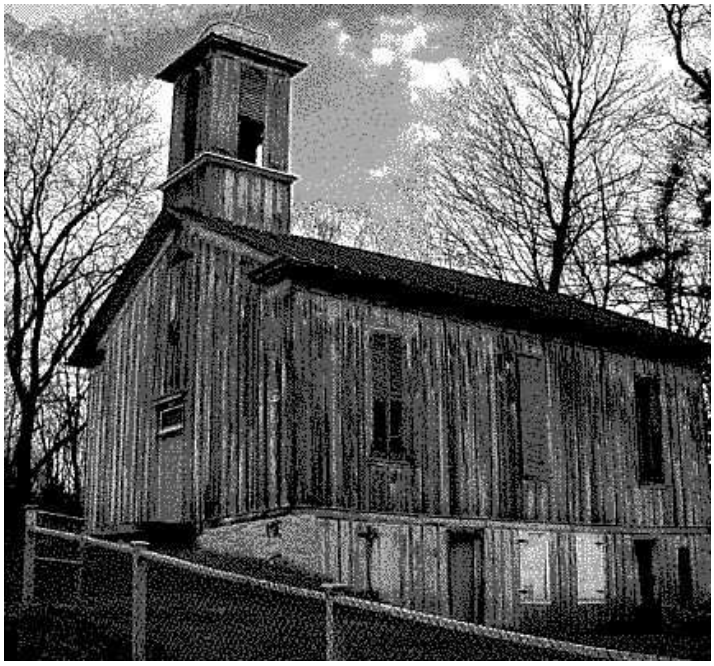

(b) Church image

Figure 3.8: Original images used for testbed

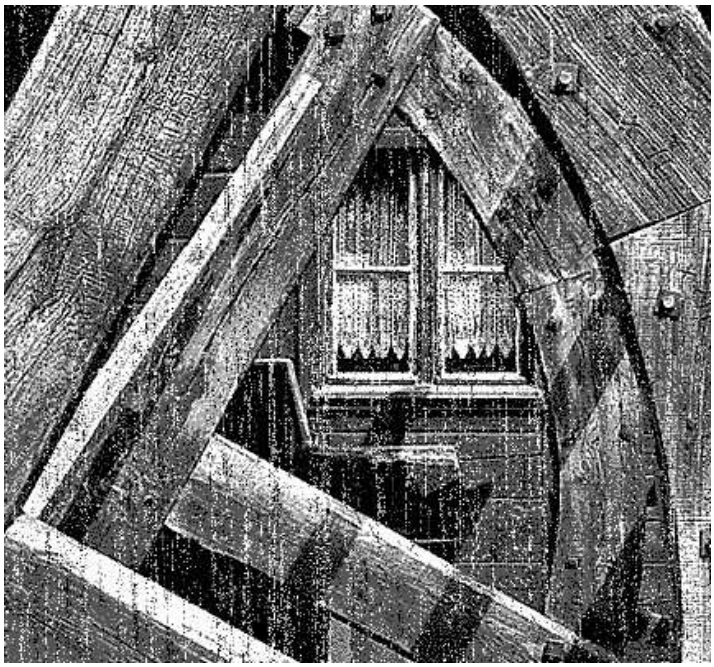

(a) Before BICM

(b) After BICM

Figure 3.9: Wood image

(a) Before BICM

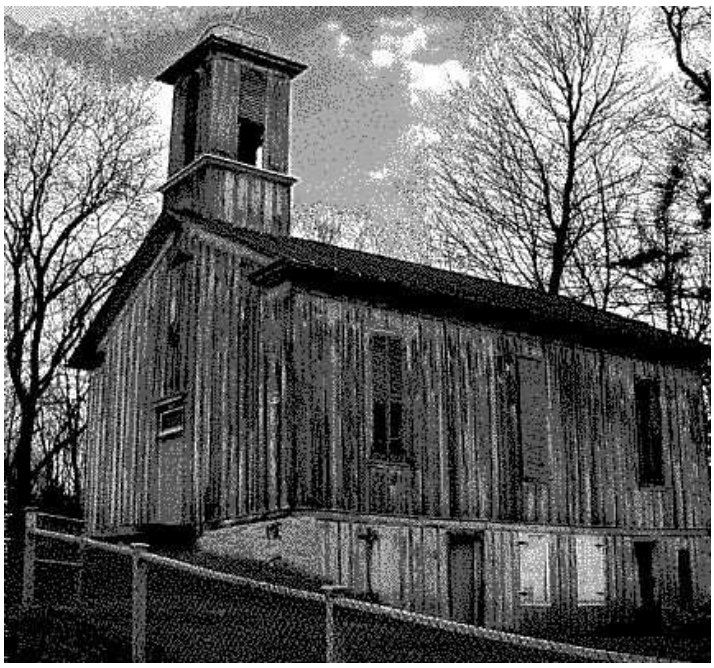

(b) After BICM

Figure 3.10: Church image

CHAPTER 4

MIMO-OFDM in Fast Fading Channels

High data-rate wireless access is demanded by many applications. Traditionally, more bandwidth is required for higher data-rate transmission. However, due to spectral limitations, it is often impractical or sometimes very expensive to increase bandwidth. In this case, using multiple transmit and receive antennas for spectrally efficient transmission is an alternative solution.

Theoretical studies of communication links employing multiple transmit and receive antennas have shown great potential [11, 12] for providing spectrally efficient wireless transmission. The early investigations focused almost entirely on flat fading channels. Recently [13], investigations have began to consider similar single-carrier approaches for frequency-selective fading channels with the hope of showing that similar gains could be achieved for mobile communications. These investigations are ultimately faced with a very complex equalization problem.

Here we consider an alternative approach, which employs multiple transmit and receive antennas in an orthogonal frequency division multiplexing (OFDM) communication system to produce what has been called a multiple-input and multiple-output (MIMO) OFDM system. MIMO-OFDM greatly lessens, and

possibly eliminates, the equalization complexity problem to produce an approach with tremendous potential.

Interchannel interference(ICI) problem still exists in MIMO-OFDM systems, however, when the channel is time-varying or when there are impairments such as synchronization errors (e.g., frequency offset). Similar to SISO-OFDM in the previous chapters, MIMO-OFDM is also sensitive to Doppler and frequency errors that destroy the subcarrier orthogonality and give rise to ICI.

The frequency domain equalization technique used for reducing ICI in SISO-OFDM systems can be applied to MIMO-OFDM systems as well. The difference is that the equalizer tries to equalize not only ICI, but the mixed signals from more than one transmit antennas, assuming that the signals from each transmit antennas are from independent sources, and the receiver can hear all the mixed signals without any orthogonality assumption among transmitted symbols. Since the ICI property, which is the interference energy is concentrated among desired subchannels, still holds with MIMO-OFDM systems, the complexity reduction method used for SISO-OFDM systems can also be applied.

In this chapter the system models for an MIMO-OFDM system under time-varying channel are derived, and the traditional MMSE approach for MIMO-OFDM systems is introduced. As an extension of the q-tap MMSE equalizer for SISO-OFDM, a similar design approach is described for q-tap MMSE equalizer for MIMO-OFDM systems. Several simulation results under various scenarios are shown.

4.1 System Model for MIMO-OFDM under a Time-Varying Channel

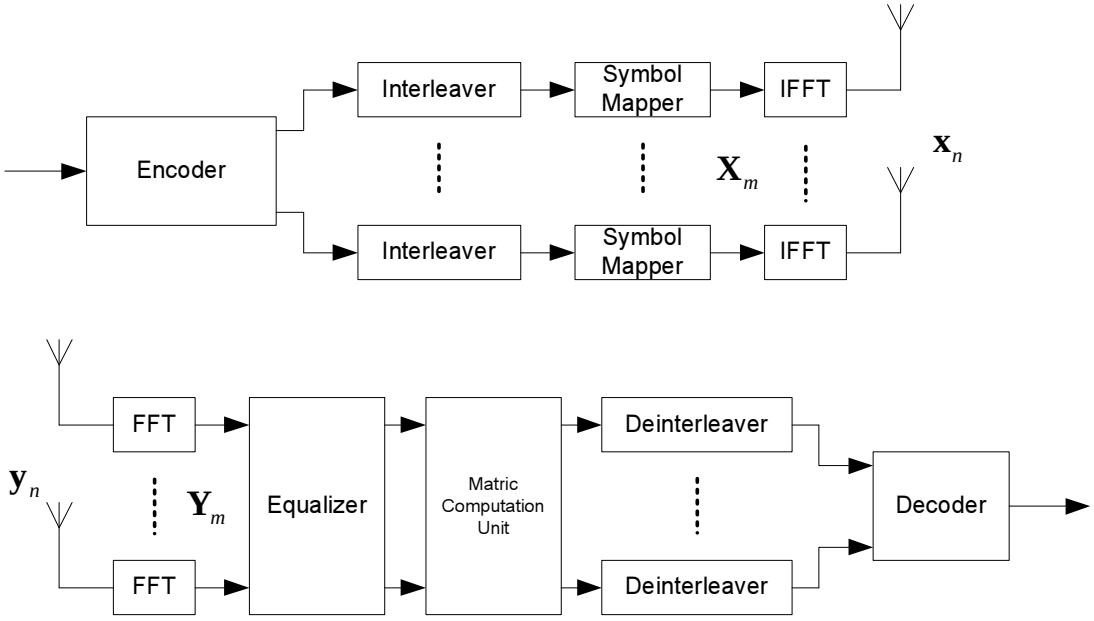

Figure 4.1: A simplified block diagram for a MIMO-OFDM system

Consider a MIMO-OFDM system using N_t transmit antennas and N_r receive antennas (Figure 4.1). The encoder takes a single stream of binary input data and transforms it into N_t parallel streams of encoded bits followed by interleavers and symbol mappers. After the symbol mappers, the mth IFFT input at transmit antenna i is denoted by X_m^i, $m = 0, \ldots, N-1$, $i = 1, \ldots, N_t$. After the IFFT, the nth OFDM symbol at transmit antenna i denoted by x_n^i is given by

$$x_n^i = \frac{1}{\sqrt{N}} \sum_{m=0}^{N-1} X_m^i e^{j2\pi nm/N}, \quad n = 0, \ldots, N-1, \quad i = 1, \ldots, N_t. \tag{4.1}$$

Here the cyclic prefix is omitted for simplicity. Let $h_{n,l}^{j,i}$ be the impulse response

of the lth multipath component at time n from transmit antenna i to receive antenna j. Then nth received symbol at receive antenna j is

$$y_n^j = \sum_{i=1}^{N_t} \sum_{l=0}^{L-1} h_{n,l}^{j,i} x_{n-l}^i + w_n^j, \quad n = 0, \ldots, N-1, \quad j = 1, \ldots, N_r, \tag{4.2}$$

where w_n^j represents additive white gaussian noise of jth receive antenna at time n. Note that y_n^j is the sum of transmitted symbols from all transmit antennas. From (4.1), y_n^j can be written as

$$\begin{aligned} y_n^j &= \frac{1}{\sqrt{N}} \sum_{i=1}^{N_t} \sum_{l=0}^{L-1} h_{n,l}^{j,i} \sum_{m=0}^{N-1} X_m^i e^{j2\pi(n-l)m/N} + w_n^j \\ &= \frac{1}{\sqrt{N}} \sum_{m=0}^{N-1} \sum_{i=1}^{N_t} X_m^i e^{j2\pi nm/N} \sum_{l=0}^{L-1} h_{n,l}^{j,i} e^{-j2\pi lm/N} + w_n^j. \end{aligned} \tag{4.3}$$

By defining

$$H_{n,(m)}^{j,i} \equiv \sum_{l=0}^{L-1} h_{n,l}^{j,i} e^{-j2\pi lm/N}, \quad n, m = 0, \ldots, N-1 \tag{4.4}$$

where $H_{n,(m)}^{j,i}$ is the Fourier transform of the channel impulse response from transmit antenna i to receive antenna j at time n. So, y_n can be rewritten as

$$y_n^j = \frac{1}{\sqrt{N}} \sum_{m=0}^{N-1} \sum_{i=1}^{N_t} X_m^i H_{n,(m)}^{j,i} e^{j2\pi nm/N} + w_n^j. \tag{4.5}$$

Since the mth FFT output at receive antenna j is given by

$$Y_m^j = \frac{1}{\sqrt{N}} \sum_{n=0}^{N-1} y_n^j e^{-j2\pi nm/N}, \quad m = 0, \ldots, N-1, \quad j = 1, \ldots, N_r, \tag{4.6}$$

we have

$$\begin{aligned} Y_m^j &= \frac{1}{\sqrt{N}} \sum_{n=0}^{N-1} \left(\frac{1}{\sqrt{N}} \sum_{k=0}^{N-1} \sum_{i=1}^{N_t} X_k^i H_{n,(k)}^{j,i} e^{j2\pi nk/N} + w_n^j \right) e^{-j2\pi nm/N} \\ &= \frac{1}{N} \sum_{k=0}^{N-1} \sum_{i=1}^{N_t} X_k^i \sum_{n=0}^{N-1} H_{n,(k)}^{j,i} e^{-j2\pi(m-k)n/N} + \frac{1}{\sqrt{N}} \sum_{n=0}^{N-1} w_n^j e^{-j2\pi nm/N} \\ &= \sum_{i=0}^{N_t} \left[\frac{1}{N} \sum_{n=0}^{N-1} H_{n,(m)}^{j,i} \right] X_m^i + \frac{1}{N} \sum_{i=1}^{N_t} \sum_{k=0,k\neq m}^{N-1} X_k^i \sum_{n=0}^{N-1} H_{n,(k)}^{j,i} e^{-j2\pi(m-k)n/N} + W_m^j \\ &= \sum_{i=1}^{N_t} \alpha_m^{j,i} X_m^i + \sum_{i=1}^{N_t} \beta_m^{j,i} + W_m^j, \end{aligned} \tag{4.7}$$

where

$$\alpha_m^{j,i} = \frac{1}{N} \sum_{n=0}^{N-1} H_{n,(m)}^{j,i}, \tag{4.8}$$

$$\beta_m^{j,i} = \sum_{k=0,k\neq m}^{N-1} X_k^i \sum_{n=0}^{N-1} H_{n,(k)}^{j,i} e^{-j2\pi(m-k)n/N}, \tag{4.9}$$

$$W_m^j = \frac{1}{\sqrt{N}} \sum_{n=0}^{N-1} w_m^j e^{-j2\pi nm/N}. \tag{4.10}$$

Similar to SISO case, $\alpha_m^{j,i}$ and $\beta_m^{j,i}$ represent the multiplicative distortion and the interchannel interference of a desired subchannel m from transmit antenna i to receive antenna j respectively, and W_m^j is the frequency response of the AWGN. Also it is easy to show that, if the channel is time-invariant, then $\alpha_m^{j,i}$, and $\beta_m^{j,i}$ become the frequency response of the subchannel m, and zero, respectively.

(4.7) can be expressed by a compact vector-matrix form as

$$\mathbf{y} = \mathbf{H}\mathbf{x} + \mathbf{w}, \tag{4.11}$$

where

$$\begin{aligned} \mathbf{y} &= \left[\mathbf{y}_0^{\mathrm{T}}, \mathbf{y}_1^{\mathrm{T}}, \ldots, \mathbf{y}_{N-1}^{\mathrm{T}}\right]^{\mathrm{T}}, \\ \mathbf{x} &= \left[\mathbf{x}_0^{\mathrm{T}}, \mathbf{x}_1^{\mathrm{T}}, \ldots, \mathbf{x}_{N-1}^{\mathrm{T}}\right]^{\mathrm{T}}, \\ \mathbf{w} &= \left[\mathbf{w}_0^{\mathrm{T}}, \mathbf{w}_1^{\mathrm{T}}, \ldots, \mathbf{w}_{N-1}^{\mathrm{T}}\right]^{\mathrm{T}}, \end{aligned} \tag{4.12}$$

and

$$\mathbf{H} = \begin{bmatrix} \mathbf{H}_{0,0} & \mathbf{H}_{0,1} & \cdots & \mathbf{H}_{0,N-1} \\ \mathbf{H}_{1,0} & \mathbf{H}_{1,1} & \cdots & \mathbf{H}_{1,N-1} \\ \vdots & \vdots & \ddots & \vdots \\ \mathbf{H}_{N-1,0} & \mathbf{H}_{N-1,1} & \cdots & \mathbf{H}_{N-1,N-1} \end{bmatrix}. \tag{4.13}$$

In (4.12),

$$\begin{aligned} \mathbf{y}_m &= \left[Y_m^1, Y_m^2, \ldots, Y_m^{N_r}\right]^{\mathrm{T}} \\ \mathbf{x}_m &= \left[X_m^1, X_m^2, \ldots, X_m^{N_t}\right]^{\mathrm{T}} \\ \mathbf{w}_m &= \left[W_m^1, W_m^2, \ldots, W_m^{N_r}\right]^{\mathrm{T}}. \end{aligned} \tag{4.14}$$

Also in (4.13),

$$\mathbf{H}_{n,m} = \begin{bmatrix} H_{n,m}^{1,1} & H_{n,m}^{1,2} & \cdots & H_{n,m}^{1,N_t} \\ H_{n,m}^{2,1} & H_{n,m}^{2,2} & \cdots & H_{n,m}^{2,N_t} \\ \vdots & \vdots & \ddots & \vdots \\ H_{n,m}^{N_r,1} & H_{n,m}^{N_r,2} & \cdots & H_{n,m}^{N_r,N_t} \end{bmatrix} \tag{4.15}$$

where each element is defined as

$$H_{n,m}^{j,i} \equiv \frac{1}{N} \sum_{n=0}^{N-1} H_{n,(m)}^{j,i} e^{-j2\pi(m-k)n/N}. \tag{4.16}$$

β_m^j's in (4.7), or off-diagonal elements of $\mathbf{H}$ in (4.13) represent the interchannel interference. In a time-invariant channel, one can easily see that β_m^j is zero, or $\mathbf{H}$ becomes a block-diagonal matrix, due to the orthogonality of the multicarrier basis waveforms. In a slowly time-varying channel, i.e., the normalized Doppler frequency f_dT is small, we can assume $E\{|\beta_m^j|^2\} \approx 0$. On the other hand, when the normalized Doppler frequency is high, the power of the ICI cannot be ignored, and the power of the desired signal is reduced.

4.2 MMSE Equalizer for MIMO-OFDM

The MMSE equalizer is one of the solutions for reducing interchannel interference as well as equalizing mixed signals transmitted from more than one transmit antennas for MIMO-OFDM systems in fast fading channels. Consider the MIMO-OFDM system model

$$\mathbf{y} = \mathbf{H}\mathbf{x} + \mathbf{w}, \tag{4.17}$$

as given in (4.11). Here we want to find the NN_t-by-NN_r equalizer matrix $\mathbf{G}$ which minimizes the cost function

$$E\left\{\|\mathbf{x} - \hat{\mathbf{x}}\|^2\right\}, \tag{4.18}$$

where $\hat{\mathbf{x}} = \mathbf{G}\mathbf{y}$ is the equalizer output vector. If the NN_r-by-NN_t channel matrix $\mathbf{H}$ is given, the solution of MMSE equalizer $\mathbf{G}$ can be obtained by the following equation:

$$\mathbf{G} = \mathbf{H}^{\mathrm{H}}\left(\mathbf{H}\mathbf{H}^{\mathrm{H}} + \frac{\sigma_w^2}{\sigma_x^2}\mathbf{I}_{NN_r}\right)^{-1}, \tag{4.19}$$

where $\mathbf{I}_{NN_r}$ is the NN_r-by-NN_r identity matrix. Also the corresponding mean-squared error is

$$\text{MMSE} = \sigma_x^2 \text{Tr}\left(\mathbf{I}_{NN_t} - \mathbf{GH}\right). \tag{4.20}$$

Similar to the SISO case, however, the traditional way of designing an MMSE equalizer for MIMO-OFDM systems in fast fading channels requires a very inefficient and highly complex structure. According to (4.19), NN_r-by-NN_r complex matrix inversion is necessary to obtain the complex equalizer matrix $\mathbf{G}$, and $N^2N_tN_r$ complex multipliers are needed to equalize NN_t symbols. Since the FFT size N is usually large number, the traditional MMSE approach should be avoided in practical applications.

4.3 q-tap MMSE Equalizer for MIMO-OFDM

The q-tap MMSE equalizer for MIMO-OFDM systems can be derived similarly to the SISO case in the previous chapter. The problem is to find the N_t by qN_r equalizer matrix $\mathbf{g}_m^{(q)}$

$$\mathbf{g}_m^{(q)} = \left[\mathbf{g}_{m,1}, \ldots, \mathbf{g}_{m,q}\right], \tag{4.21}$$

which minimizes the mean-squared error function,

$$E\left\{\left\|\mathbf{x}_m - \hat{\mathbf{x}}_m\right\|^2\right\}, \tag{4.22}$$

where $\mathbf{g}_m^{(q)}$ is N_t by N_r equalizer matrix of mth subchannel,

$$\hat{\mathbf{x}}_m = \mathbf{g}_m^{(q)} \mathbf{y}_m^{(q)}, \tag{4.23}$$

and

$$\mathbf{y}_m^{(q)} = \left[\mathbf{y}_{(m-(q-1)/2)_N}^{\mathrm{T}}, \ldots, \mathbf{y}_m^{\mathrm{T}}, \ldots, \mathbf{y}_{(m+(q-1)/2)_N}^{\mathrm{T}}\right]^{\mathrm{T}}. \tag{4.24}$$

Here $(\cdot)_N$ denotes modular function with modulus N. Thus $\mathbf{y}_m^{(q)}$ is then

$$\mathbf{y}_m^{(q)} = \mathbf{H}_m^{(q)}\mathbf{x} + \mathbf{w}_m^{(q)}, \tag{4.25}$$

where

$$\mathbf{H}_m^{(q)} = \begin{bmatrix} \mathbf{H}_{(m-(q-1)/2)_N,0} & \mathbf{H}_{(m-(q-1)/2)_N,1} & \cdots & \mathbf{H}_{(m-(q-1)/2)_N,N-1} \\ \vdots & \vdots & \vdots & \vdots \\ \mathbf{H}_{m,0} & \mathbf{H}_{m,1} & \cdots & \mathbf{H}_{m,N-1} \\ \vdots & \vdots & \vdots & \vdots \\ \mathbf{H}_{(m+(q-1)/2)_N,0} & \mathbf{H}_{(m+(q-1)/2)_N,1} & \cdots & \mathbf{H}_{(m+(q-1)/2)_N,N-1} \end{bmatrix}, \tag{4.26}$$

and

$$\mathbf{w}_m^{(q)} = \left[\mathbf{w}_{(m-(q-1)/2)_N}^{\mathrm{T}}, \ldots, \mathbf{w}_m^{\mathrm{T}}, \ldots, \mathbf{w}_{(m+(q-1)/2)_N}^{\mathrm{T}}\right]^{\mathrm{T}}. \tag{4.27}$$

The MMSE solution can be obtained by the following equation:

$$\mathbf{g}_m^{(q)} = \mathbf{R}_{\mathbf{x}_m\mathbf{y}_m^{(q)}}\mathbf{R}_{\mathbf{y}_m^{(q)}}^{-1}. \tag{4.28}$$

Using the same assumption in the previous chapter, we have

$$\begin{aligned} \mathbf{R}_{\mathbf{x}_m\mathbf{y}_m^{(q)}} &= E\left\{\mathbf{x}_m\left(\mathbf{y}_m^{(q)}\right)^{\mathrm{H}}\right\} \\ &= E\left\{\mathbf{x}_m\left(\mathbf{H}_m^{(q)}\mathbf{x} + \mathbf{w}_m^{(q)}\right)^{\mathrm{H}}\right\} \\ &= E\left\{\mathbf{x}_m\mathbf{x}^{\mathrm{H}}\right\}\left(\mathbf{H}_m^{(q)}\right)^{\mathrm{H}} \\ &= \sigma_x^2\left(\mathbf{h}_m^{(q)}\right)^{\mathrm{H}}, \end{aligned} \tag{4.29}$$

where $\mathbf{h}_m^{(q)}$ is the mth column of the matrix $\mathbf{H}_m^{(q)}$, i.e.,

$$\mathbf{h}_m^{(q)} = \left[\mathbf{H}^{\mathrm{T}}_{(m-(q-1)/2)_N,m}, \ldots, \mathbf{H}^{\mathrm{T}}_{m,m}, \ldots, \mathbf{H}^{\mathrm{T}}_{(m+(q-1)/2)_N,m}\right]^{\mathrm{T}}. \tag{4.30}$$

Also we have

$$\begin{aligned}
\mathbf{R}_{\mathbf{y}_m^{(q)}} &= E\left\{\mathbf{y}_m^{(q)}\left(\mathbf{y}_m^{(q)}\right)^{\mathrm{H}}\right\} \\
&= E\left\{\left(\mathbf{H}_m^{(q)}\mathbf{x} + \mathbf{w}_m^{(q)}\right)\left(\mathbf{H}_m^{(q)}\mathbf{x} + \mathbf{w}_m^{(q)}\right)^{\mathrm{H}}\right\} \\
&= \mathbf{H}_m^{(q)} E\left\{\mathbf{x}\mathbf{x}^{\mathrm{H}}\right\}\left(\mathbf{H}_m^{(q)}\right)^{\mathrm{H}} + E\left\{\mathbf{w}_m^{(q)}\left(\mathbf{w}_m^{(q)}\right)^{\mathrm{H}}\right\} \\
&= \sigma_x^2 \mathbf{H}_m^{(q)}\left(\mathbf{H}_m^{(q)}\right)^{\mathrm{H}} + \sigma_w^2 \mathbf{I}_{qN_r}.
\end{aligned} \tag{4.31}$$

Thus the q-tap equalizer matrix $\mathbf{g}_m^{(q)}$ is

$$\mathbf{g}_m^{(q)} = \left(\mathbf{h}_m^{(q)}\right)^{\mathrm{H}}\left(\mathbf{H}_m^{(q)}\left(\mathbf{H}_m^{(q)}\right)^{\mathrm{H}} + \frac{\sigma_w^2}{\sigma_x^2}\mathbf{I}_{qN_r}\right)^{-1}. \tag{4.32}$$

Similarly, we have

$$\mathrm{MMSE} = \sigma_x^2 \sum_{m=0}^{N-1} \mathrm{Tr}\left(\mathbf{I}_{N_t} - \mathbf{g}_m^{(q)}\mathbf{h}_m^{(q)}\right). \tag{4.33}$$

The dimension of the covariance matrix $\mathbf{R}_{\mathbf{y}_m^{(q)}}$ in (4.31) is qN_r-by-qN_r. If we chose q small enough, and the number of the receive antennas is reasonably small, the inversion of $\mathbf{R}_{\mathbf{y}_m^{(q)}}$ is not a very hard task in hardware, considering today's technology. For example, when $q = 3$, $N_t = 2$, and $N_r = 2$, 6-by-6 matrix inversion with 2-by-6 matrix multiplications per subchannel are required, which are quite modest operations in most digital signal processors today.

4.4 Simulation Results

Figure 4.2 shows the mean-squared error (MSE) performance of MMSE equalizers with two transmit antennas when the normalized Doppler frequency is 0.1. In these simulations 64 subchannels are used for OFDM. Figure 4.2(a) demonstrates the theoretical limits on the MSE performance of the MMSE equalizer for different number of receive antennas, i.e. 1, 2, and 3 antennas. Examining Figure 4.2(a), the MSE performance of the equalizer degrades dramatically, when the number of receive antennas is less than the transmit antennas. In a mathematical point of view, N_r should be greater than or equal to N_t, in order to obtain a proper MMSE solution. However, there are situations where N_r must be less than N_t due to the physical limitations of receivers, such as mobile handsets. In such cases, orthogonal coding, such as Alamouti code [14], should be applied to transmit symbols from each transmit antenna in order to avoid performance degradation. Figure 4.2(b) compares the MSE performances of single-tap, 3-tap, and full-tap (64-tap) MMSE equalizers. The overall performance can be much improved by adding one more receive antenna. The performance of 3-tap MMSE is somewhere in the middle between single-tap and full-tap MMSE equalizers. In the low SNR region, small-tap MMSE equalizers work relatively well, but the curves become virtually flat as the SNR increases, due to the irreducible error floor, which has not been equalized by small-tap equalizers.

Figure 4.3 shows the MSE performance of MMSE equalizers employing four transmit antennas when the normalized Doppler frequency is 0.1. Examining

Figure 4.3(a), the overall performance is worse than the 2× system of which the throughput is half that of the 4× system. It is interesting to see that the error floor levels of 3-tap equalizers in Figure 4.3(b) are higher than 2× systems in Figure 4.2(b). This is because the sum of remaining ICI terms from all transmit antennas increases linearly as the number of transmit antennas.

Figure 4.4, and 4.5 show the MSE performance of MMSE equalizers with two and four transmit antennas, respectively, when the normalized Doppler frequency is 0.2. Similar results can be observed except the performance gaps between full-tap and small-tap equalizers become larger, due to higher Doppler frequency.

4.5 Summary

In this chapter the multiple-input multiple-output (MIMO) OFDM system in fast fading channels was explored as an extension of Chapter 2. The mathematical model for the MIMO-OFDM was derived. The difference from the single-input single-output (SISO) case in Chapter 2 is that the MIMO system requires additional processing for the mixed signals from several transmit antennas. The MMSE equalizer was suggested for equalizing both the ICI and the mixed signals. Again, since the traditional MMSE approach is impractical, especially for MIMO systems, new q-tap MMSE equalizer was designed using the ICI property described in Chapter 2. Several simulation results confirmed that the q-tap MMSE equalizer for MIMO-OFDM systems works well under various scenarios.

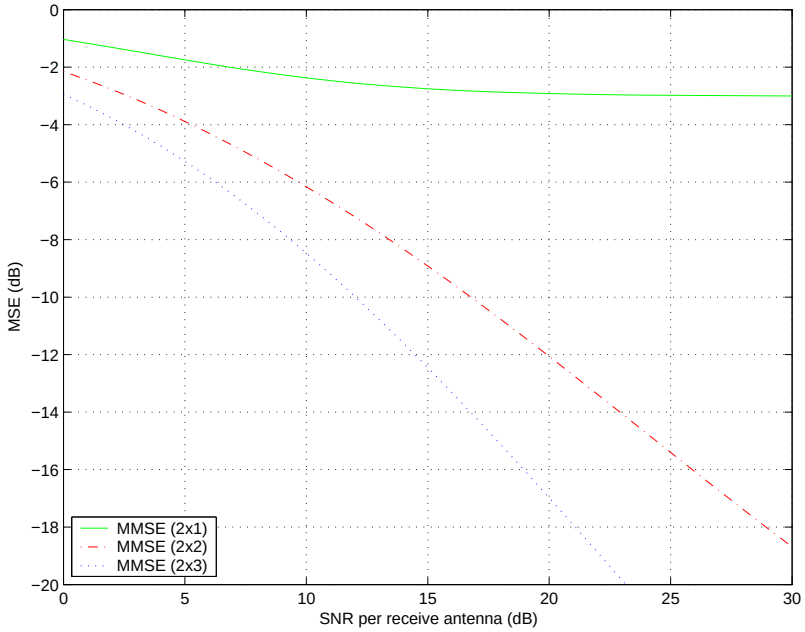

(a) Different antenna configuration

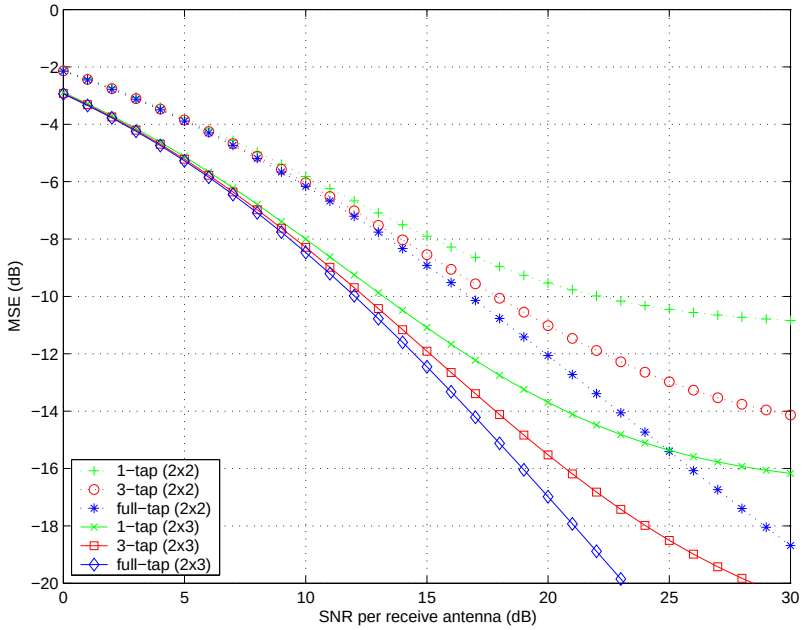

(b) q-tap MMSE performance

Figure 4.2: MSE performance of MMSE equalizers for 2x systems, $f_dT = 0.1$

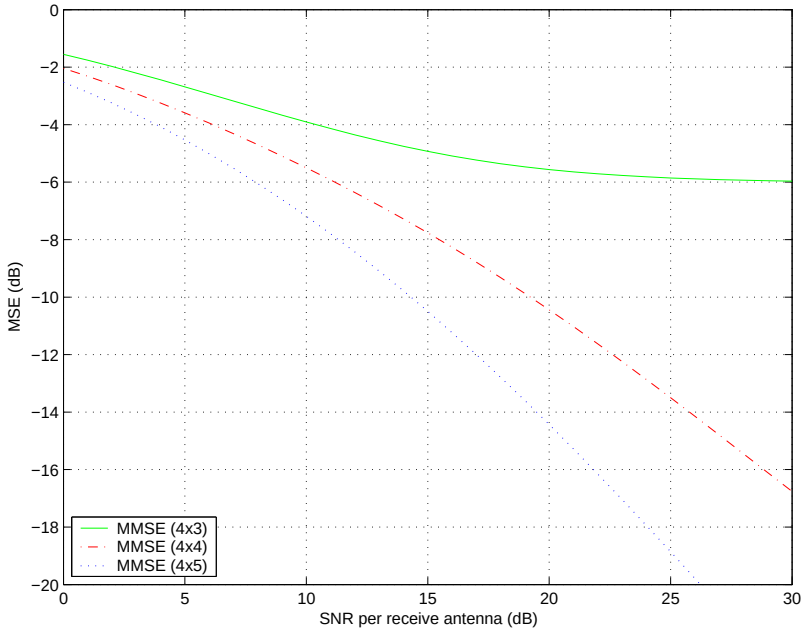

(a) Different antenna configuration

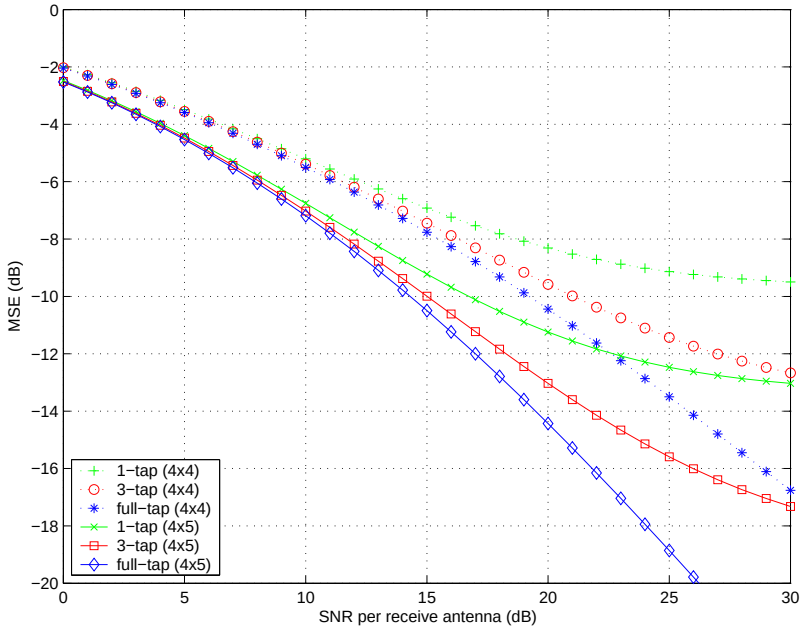

(b) q-tap MMSE performance

Figure 4.3: MSE performance of MMSE equalizers for 4x systems, $f_dT = 0.1$

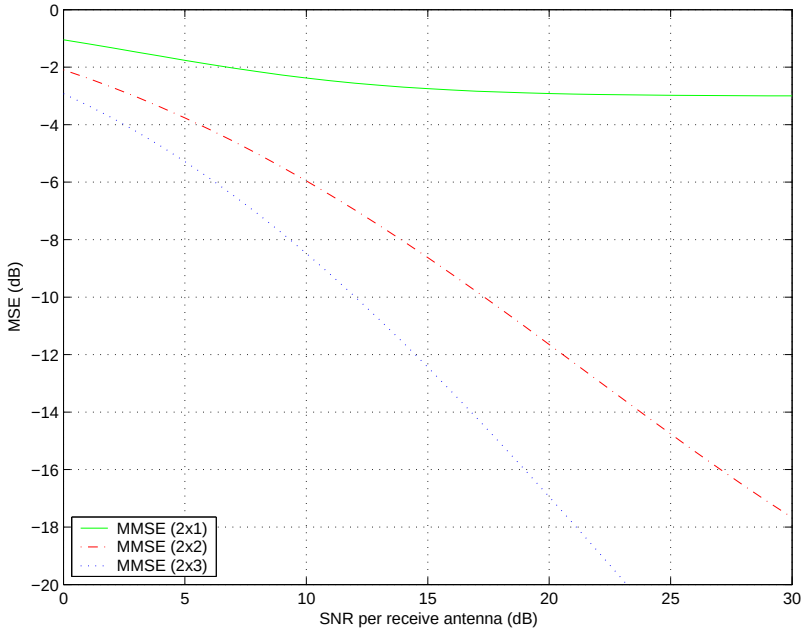

(a) Different antenna configuration

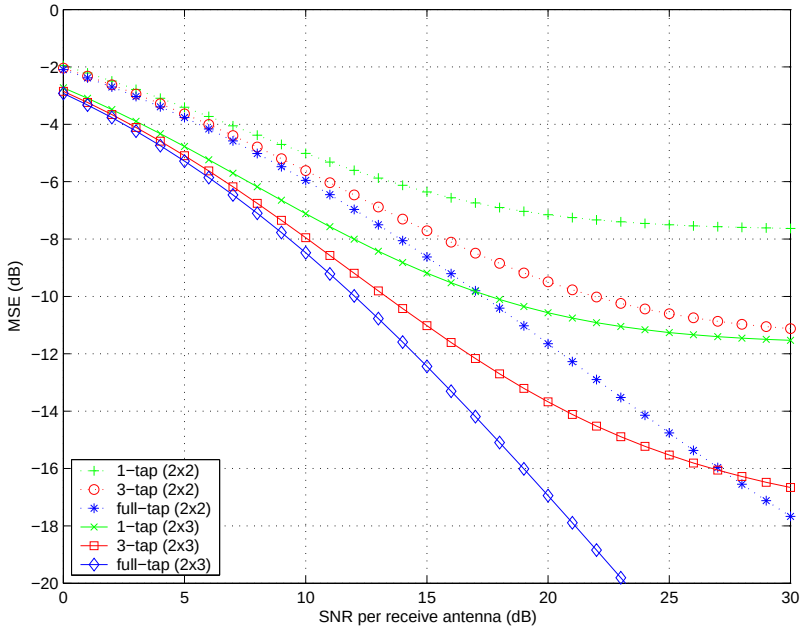

(b) q-tap MMSE performance

Figure 4.4: MSE performance of MMSE equalizers for 2x systems, $f_dT = 0.2$

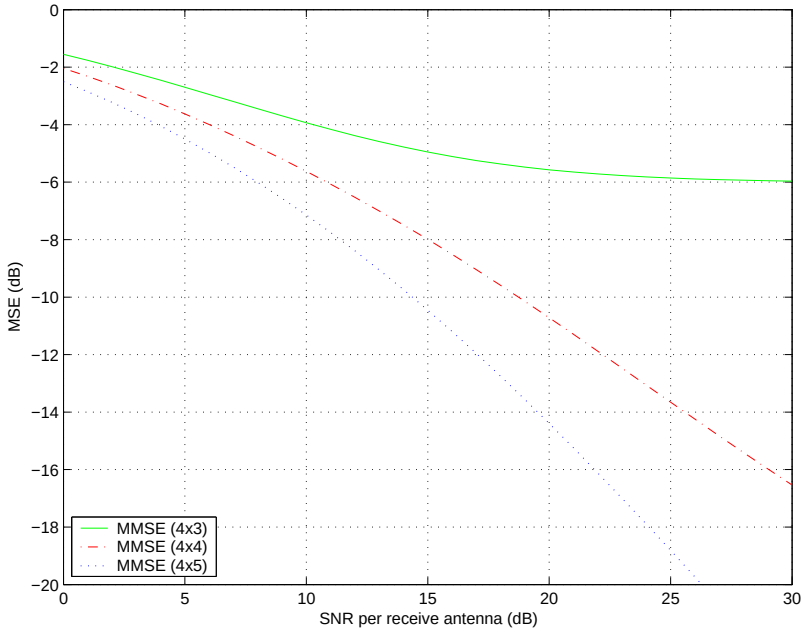

(a) Different antenna configuration

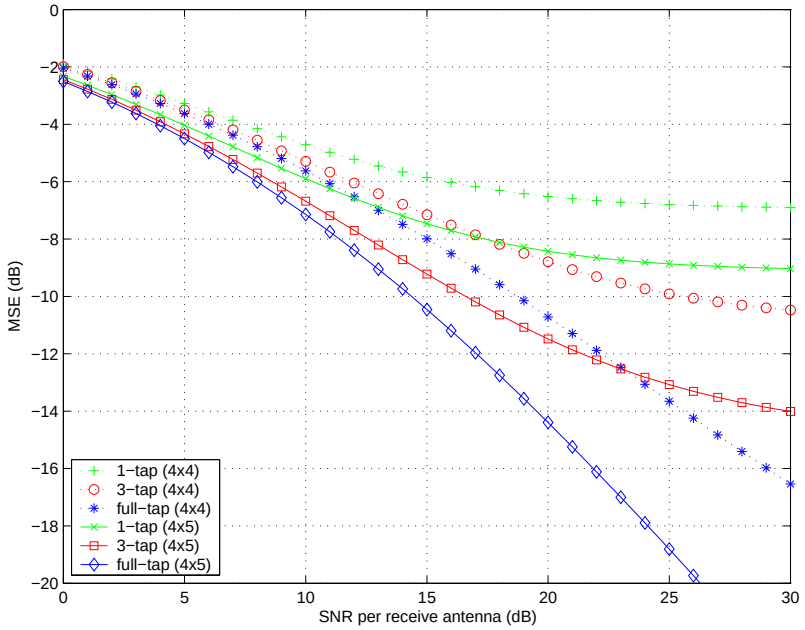

(b) q-tap MMSE performance

Figure 4.5: MSE performance of MMSE equalizers for 4x systems, $f_dT = 0.2$

CHAPTER 5

Channel Coding for MIMO-OFDM in Fast Fading Channels

Channel coding for wireless communications equipment with transmit and receive diversity is a fairly new field of research [15, 16]. Performance limits in terms of outage capacity are derived in [11] for the quasi-static fading channel, whereas [17] also covers the capacity for the ergodic fast fading channels.

Space-time trellis codes (STCs) [12,18,19] are well suited for multiple antenna transmission systems with a quasi-static fading (e.e., block-fading) environment, but our ultimate aim is to apply coding to OFDM systems [5, 20–22]. We need to realize that the channel characteristic across subcarriers in OFDM does not comply with the widely used quasi-static channel model. Adjacent channel coefficients are not independent, but together with frequency interleaving within one OFDM symbol, the resulting channel characteristics can be approximated by an independent fast fading channel model.

Obviously, we need to reconsider the channel coding problem in OFDM systems to make best use of exploitable frequency diversity of the transformed multipath channel. Multidimensional signal sets are introduced in [23] to increase

the diversity factor in OFDM. Recent progress has been made for the multiple antenna case by optimizing STCs for fast fading [24–26] or by applying the idea of I-Q (inphase and quadrature component) interleaving to STCs [27,28]. We will not investigate the latter method because it also increases diversity in bit-based coding [29]. The question remains as to whether or not STCs are an appropriate channel coding class for MIMO-OFDM systems in fast fading scenarios.

In this chapter we compare STCs and BICM for multiple antenna scenarios with fast – or at least faster than quasi-static – fading conditions. Then we combine the channel coding with q-tap MMSE equalizers, designed in the previous chapter. New decoding metrics are developed to accommodate the channel coding with the equalizers. The metrics can be used for both STCs and BICM.

5.1 Space-Time Coding

Space-time codes have attracted considerable attention recently [1, 12–14, 18, 19, 24–26, 30–38] as a useful approach for increasing the performance of wireless communication systems by using multiple transmit antennas. Information theory has been used to demonstrate that multiple antennas have the potential to dramatically increase achievable bit rates [39], thus converting wireless channels from narrow to wide data pipes. Space-time codes realize these gains by introducing temporal and spatial correlation into the signals transmitted from different antennas without increasing the total transmitted power or transmission bandwidth. There is in fact a diversity gain that results from multiple paths between the

base station and user terminal, and a coding gain that results from how symbols are correlated across transmit antennas. Significant increases in throughput are possible with only two antennas at the base station and one or two antennas at the user terminal, and with simple receiver structures. The second antenna at the user terminal can be used to further increase system capacity through interference suppression.

STC enjoys several advantages that make it very attractive for high-rate wireless applications. First, it improves the downlink performance (which is the bottleneck in asymmetric applications such as Internet browsing and downloading) without the need for multiple receive antennas at the terminals (which are required to have low cost and a small form factor). Second, it elegantly combines spatial transmit diversity with channel coding (as shown in [12]) realizing a coding gain in addition to maximum diversity gain. Third, it does not require channel state information (CSI) at the transmitter, and by operating open loop, it eliminates the need for an expensive reverse link that may also be unreliable in the case of rapid channel fading. Finally, it has been shown to be robust against non-ideal operating conditions such as antenna correlation, channel estimation errors, and Doppler effects [18].

Successful implementation of STC over multi-user broadband frequency-selective channels requires the development of novel, practical, and high-performance signal processing algorithms for channel estimation, joint equalization/decoding, and interference suppression. This task is quite challenging due to the long delay spread of broadband channels, which increases the number of channel parameters

to be estimated and the number of trellis states in joint equalization/decoding, especially with multiple transmit antennas. This, in turn, places significant additional computation and power consumption loads on user terminals. On the other hand, development and implementation of such advanced algorithms for broadband wireless channels promises even more significant performance gains than those reported for narrowband channels due to availability of multipath (in addition to spatial) diversity gains that can be utilized.

Initial STC research efforts focused on narrowband flat-fading channels [12, 14,18]. Based on the performance measures given in [12,33], optimum quasi-static space-time convolutional codes are defined in [12] to be those which achieve the highest coding gain of those codes achieving maximum diversity gain. More recently, a number of authors have attempted brute-force searches for codes optimizing this criterion [35, 37, 38].

An example of a 2×2 STC system is sketched in Figure 5.1. Binary information enters the STC, and in each time step, a complex-valued symbol for each antenna is generated according to a code trellis in such a fashion that the diversity and/or coding gain is maximized. The signal constellations used in all transmit antennas are identical and denoted by $\mathcal{A}$. The space-time decoder directly operates on the vector of received signal-space samples to estimate the most likely transmitted information sequence of binary decisions. Assuming that y_m^j is the received signal at receive antenna j at time m, and $\alpha_{i,j}$ is the channel gain from transmit antenna i to receive antenna j, the branch metric for a transition labeled

$x_m^1 x_m^2 \cdots x_m^{N_t}$ is given by [12]

$$\sum_{j=1}^{N_r} \left| y_m^j - \sum_{i=1}^{N_t} \alpha_{i,j} x_m^i \right|^2 . \tag{5.1}$$

Using our notations and assuming the channel is quasi-static, (5.1) can be rewritten as the following compact matrix vector form:

$$\left\| \mathbf{y}_m - \mathbf{H}_{m,m} \mathbf{x} \right\|^2 , \tag{5.2}$$

where $\mathbf{y}_m$ and $\mathbf{H}_{m,m}$ are defined in (4.14) and (4.15).

In [1], techniques for finding codes optimizing the diversity gain and the coding gain criterion suggested in [12] are presented. These techniques are based on some simple upper and lower bounds on coding gain. Also the author in [1] has shown that the codes found using these techniques have larger coding gain than some "hand designed" codes given in [12, 18, 19]. As an example, optimum q-state codes for 2 b/s/Hz with 4-QAM STCs are given in Table 5.1.

5.2 Space-Time BICM

The basic idea of BICM [40] can be extended to multiple antenna transmission [41, 42] to obtain advantages in fast fading channels. Figure 5.2 illustrates an example of the coding architecture that is used in [41], where again bold lines indicate complex values, whereas finer lines represent binary values or metrics for them. In this example, 2 transmit and 2 receive antennas with a 4-QAM constellation are used. A single convolutional code is used to encode the information bits. The coded bits are cyclically demultiplexed into the transmit branches, where they

are bit-interleaved by different-length interleavers, mapped via Gray labeling onto the signal constellation $\mathcal{A}$ used in all transmit branches, and modulated by the OFDM transmitter. For simplicity of the analysis, let us assume the channel is quasi-static, i.e. no ICI. Since there is no ICI, the received signal after the OFDM receiver is given by

$$\mathbf{y}_m = \mathbf{H}_{m,m}\mathbf{x}_m + \mathbf{w}_m \quad m = 0, \ldots, N-1 \tag{5.3}$$

where each variable is defined in (4.14) and (4.15). In the receiver, bit metrics are calculated independently for each bit, ignoring the values of other bits in this vector. The bit metrics are deinterleaved an multiplexed into one stream, which is decoded by a conventional soft-input Viterbi algorithm.

The decoding scheme of the SISO BICM system in the previous chapter can also be extended to the ST-BICM system. Here we need to define the new extended subset $\mathbf{S}_i^c$, of which the dimension is N_t. The extended subset $\mathbf{S}_i^c$ consists of the subset S_i^c and $\mathcal{A}$. For example, for the 4 transmit antenna system,

$$\mathbf{S}_i^c = S_i^c \times \mathcal{A} \times \mathcal{A} \times \mathcal{A} \tag{5.4}$$

Then the bit metric for the ST-BICM is

$$\begin{gathered} m_{n_t,i}\left(\mathbf{y}_m, \mathbf{S}_i^c; \mathbf{H}_{m,m}\right) = \min_{\mathbf{x}\in\mathbf{S}_i^c} \left\|\mathbf{y}_m - \mathbf{H}_{m,m}\mathbf{x}\right\|^2, \\ c = 0, 1, \quad i = 1, \ldots, N_b, \quad n_t = 1, \ldots, N_t, \end{gathered} \tag{5.5}$$

where $m_{n_t,i}$, and $N_b = \log_2 \|\mathcal{A}\|$ represent the bit metric for n_t transmit antenna at ith bit position, and the number of bits per symbol respectively. Each $m_{n_t,i}$ produces two bit metrics corresponding to the two possible values of the bit, 0

and 1. Hence the number of bit metrics required at each time m is $2N_tN_b$. The bit metrics are then deinterleaved, and the branch metrics for the Viterbi decoder are calculated using the following equation:

$$\begin{aligned} m\left(\mathbf{y}_m, \mathbf{c}_m; \mathbf{H}_{m,m}\right) = \sum_{n_t=1}^{N_t} \sum_{i=1}^{N_b} \left(1 - c_{m,i}^{n_t}\right) m_{n_t,i}\left(\mathbf{y}_m, \mathbf{S}_i^{c_{m,i}^{n_t}}; \mathbf{H}_{m,m}\right) \\ + c_{m,i}^{n_t} m_{n_t,i}\left(\mathbf{y}_m, \mathbf{S}_i^{c_{m,i}^{n_t}}; \mathbf{H}_{m,m}\right), \end{aligned} \tag{5.6}$$

where $c_{m,i}^{n_t}$ denotes the binary code for n_tth transmit antenna at ith bit position at time m, and

$$\mathbf{c}_m = \left(c_{m,1}^1, \ldots, c_{m,N_b}^1, \ldots\ldots, c_{m,1}^{N_t}, \ldots, c_{m,N_b}^{N_t}\right), \quad c_{m,i}^{n_t} = 0, 1. \tag{5.7}$$

Thus the total number of branch metrics required at each time m is $2^{N_bN_t}$.

Since $\|\mathcal{A}\| = 2^{N_b}$, the complexity of the bit metric computation is $\sim \|\mathcal{A}\|^{N_t}$ and rises exponentially with N_t. An important advantage of ST-BICM over STCs is large flexibility in terms of antenna reconfiguration, the size of signal constellation, and code rate. Since ST-BICM uses a single convolutional encoder with bit-based interleaving, the number of antennas and symbol mapper can be changed without any difficulties. Also, via the underlying and well-known convolutional codes, the effective coding rate can be adapted in fine-grained steps by the use of actual rate-k/m convolutional codes or by puncturing of a mother code of rate $1/m$. On the other hand, STCs require designing new codes when changing any of these parameters.

5.3 Channel Coding with q-tap MMSE Equalizer for MIMO-OFDM

One of the important reasons for employing OFDM in MIMO systems under frequency-selective fading channels is to avoid a complex equalization problem which can be greatly lessened or possibly eliminated by OFDM [25]. This is true as far as the channels are quasi-static, or slowly fading, which is not always the case. In fast fading channels, the ICI can be the bottleneck for establishing reliable wireless links between transceivers employing MIMO-OFDM. Very recently [17], investigations have began to consider fast fading scenarios, where the frequency selective channels are no longer assumed to be quasi-static. Space-time codes and proper decoding schemes can be an answer to this problem, but again, these schemes can face very complex equalization or decoding problems. Single-carrier approaches for frequency selective channels have similar problems.

The previous chapter has shown that robustness of SISO-OFDM systems in fast fading scenarios can be achieved by the combination of q-tap MMSE equalizers with BICM. This scheme can also be extended to the MIMO-OFDM systems as well. Without the equalization, the path metrics for STCs are

$$M_0^{\mathrm{STC}} \equiv \|\mathbf{y}_m - \mathbf{H}_{m,m}\mathbf{x}\|^2 , \tag{5.8}$$

as given in (5.2). Also the bit metrics for ST-BICM are

$$M_0^{\mathrm{BICM}} = \min_{\mathbf{x}\in\mathbf{S}_i^c} \|\mathbf{y}_m - \mathbf{H}_{m,m}\mathbf{x}\|^2 , \tag{5.9}$$

as given in (5.5). In the presence of equalizers, however, M_0's cannot be used

directly since we need to find the expressions of the metrics using the equalizer outputs $\hat{\mathbf{x}}_m$. The simplest forms are the ones using $\hat{\mathbf{x}}_m$ instead of $\mathbf{y}_m$, so

$$M_1^{\text{STC}} \equiv \left\|\hat{\mathbf{x}}_m - \mathbf{x}\right\|^2, \tag{5.10}$$

$$M_1^{\text{BICM}} \equiv \min_{\mathbf{x}\in\mathbf{S}_i^c} \left\|\hat{\mathbf{x}}_m - \mathbf{x}\right\|^2. \tag{5.11}$$

Examine the equalizer outputs,

$$\begin{aligned} \hat{\mathbf{x}}_m &= \mathbf{g}_m^{(q)}\mathbf{y}_m^{(q)} \\ &= \mathbf{g}_m^{(q)}\left(\mathbf{H}_{m,m}^{(q)}\mathbf{x}_m + \mathbf{w}_m^{(q)}\right) \\ &= \mathbf{g}_m^{(q)}\mathbf{h}_m^{(q)}\mathbf{x}_m + \mathbf{g}_m^{(q)}\left(\mathbf{w}_m^{(q)} + \mathbf{w}_m^{(q)\prime}\right), \end{aligned} \tag{5.12}$$

where

$$\mathbf{w}_m^{(q)\prime} = \mathbf{g}_m^{(q)}\mathbf{y}_m^{(q)} - \mathbf{g}_m^{(q)}\mathbf{h}_m^{(q)}\mathbf{x}_m \tag{5.13}$$

is the residual ICI component after the equalizer, which is assumed as Gaussian noise. Since

$$\begin{aligned} \left\|\hat{\mathbf{x}}_m - \mathbf{g}_m^{(q)}\mathbf{h}_m^{(q)}\mathbf{x}_m\right\|^2 &= \left\|\mathbf{g}_m^{(q)}\left(\mathbf{w}_m^{(q)} + \mathbf{w}_m^{(q)\prime}\right)\right\|^2 \\ &\simeq \left\|\mathbf{g}_m^{(q)}\right\|^2 \left\|\mathbf{w}_m^{(q)} + \mathbf{w}_m^{(q)\prime}\right\|^2 \end{aligned} \tag{5.14}$$

new metrics are

$$M_2^{\text{STC}} \equiv \frac{1}{\left\|\mathbf{g}_m^{(q)}\right\|^2}\left\|\hat{\mathbf{x}}_m - \mathbf{g}_m^{(q)}\mathbf{h}_m^{(q)}\mathbf{x}\right\|^2, \tag{5.15}$$

$$M_2^{\text{BICM}} \equiv \frac{1}{\left\|\mathbf{g}_m^{(q)}\right\|^2}\min_{\mathbf{x}\in\mathbf{S}_i^c}\left\|\hat{\mathbf{x}}_m - \mathbf{g}_m^{(q)}\mathbf{h}_m^{(q)}\mathbf{x}\right\|^2. \tag{5.16}$$

5.4 Simulation Results

The channels used in the simulations are based on Clarke's model with exponentially decaying power profile. The number of tones of OFDM is 64, and the guard interval is longer than the channel delay. A rate 1/2, 32-state convolutional code is used for ST-BICM, and 32-state STCs given in Table 5.1 is used for STC system. All systems have 2×2 antennas with 4-QAM constellation.

Figure 5.3, 5.4 show the BER performance of 2×2 ST-BICM system in quasi-static Rayleigh fading channels. Examining 5.3, 2×2 with 4-QAM and 1×2 with 16-QAM systems show almost identical error performances, even though transmit diversity order of 1×2 antenna is less than 2×2 antenna. This result shows that the transmit diversity mainly comes from the bit-interleaved codes, not the number of transmit antennas. This argument, however, may not be true if the interleaving length is not long enough for the channels to fade independently. Also examining Figure 5.3, the performance of 2×1 with 4-QAM is worse than 1×1 with 16-QAM, simply due to the lack of receive antenna for 2×1 with 4-QAM. Similar results can be found in Figure 5.4, as the error performance of 1×2 with 64-QAM is very close to the error performance of 3×2 with 4-QAM.

Figure 5.8 shows the bit-error performance of STCs and ST-BICM in quasi-static Rayleigh fading channels. As expected, the curve of 2×2 ST-BICM with 4-QAM is very close to the curve of 1×2 ST-BICM with 16-QAM. Overall the performance of STCs is better than ST-BICM, but they become closer as SNR increases.

Figure 5.6-5.8 show the bit-error performance of 2×2 STCs and 2×2 ST-BICM with q-tap MMSE equalizer when the normalized Doppler frequency is 0.2. For M_2 curves at 10^{-5} BER in STCs Figure 5.6, 2.5dB gain is achieved by using 3-tap equalizer, and for 3-tap curves at 10^{-5}, 3dB gain is achieved by using M_2. Examining ST-BICM Figure 5.7, 3-tap equalizer gives 3dB gain for M_2 curves at 10^{-5}, and M_2 gives 3dB gain for 3-tap curves at 10^{-5}. Figure 5.8 shows the comparison between STCs and ST-BICM. Overall, the bit-error performance of STCs seems to be better in low SNR, but the performance difference between STCs and ST-BICM become smaller as SNR increases.

5.5 Summary

In this chapter space-time convolutional codes (STCs) and space-time BICM (ST-BICM) were compared. Both coding schemes can be used for MIMO-OFDM systems. Decoding methods for STCs and ST-BICM systems under quasi-static Rayleigh channels were derived. As an extension of Chapter 3, new metrics for both STCs and ST-BICM systems were suggested, in order to combine the channel coding with the q-tap MMSE equalizer designed in Chapter 4.

ST-BICM is very flexible in design, in terms of the number of antennas, the size of signal constellation, and code rate. On the other hand, for STCs, new codes must be designed to optimize the codes for a particular setup. Overall performance of the STCs is superior to the ST-BICM, but the performance difference becomes smaller as SNR increases.

Simulation results showed that, for both STCs and ST-BICM, new suggested metrics and 3-tap MMSE equalizers provide 2-3 dB gain at 10^{-5} bit error rate.

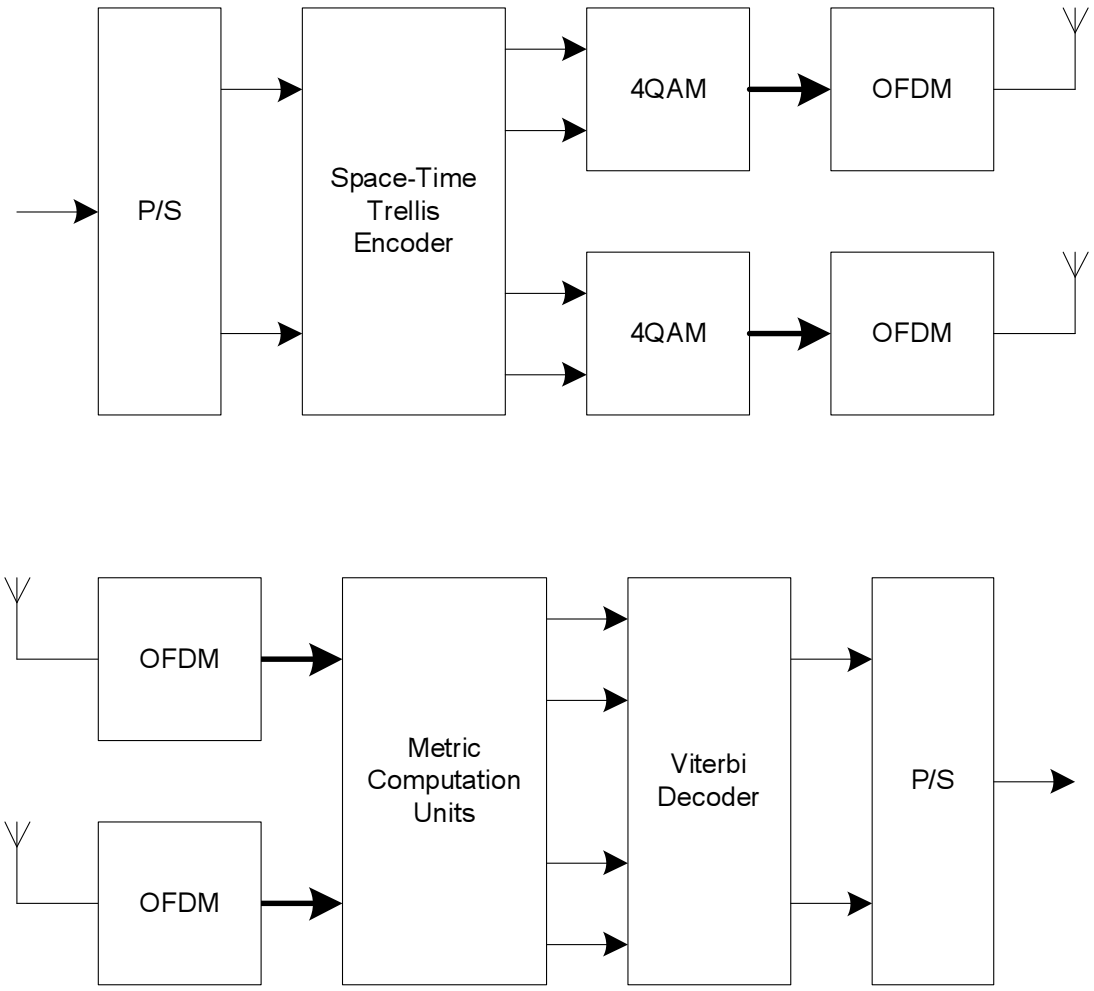

Figure 5.1: An example of transmitter and receiver in a 2×2 STCs system with 4-QAM mapping

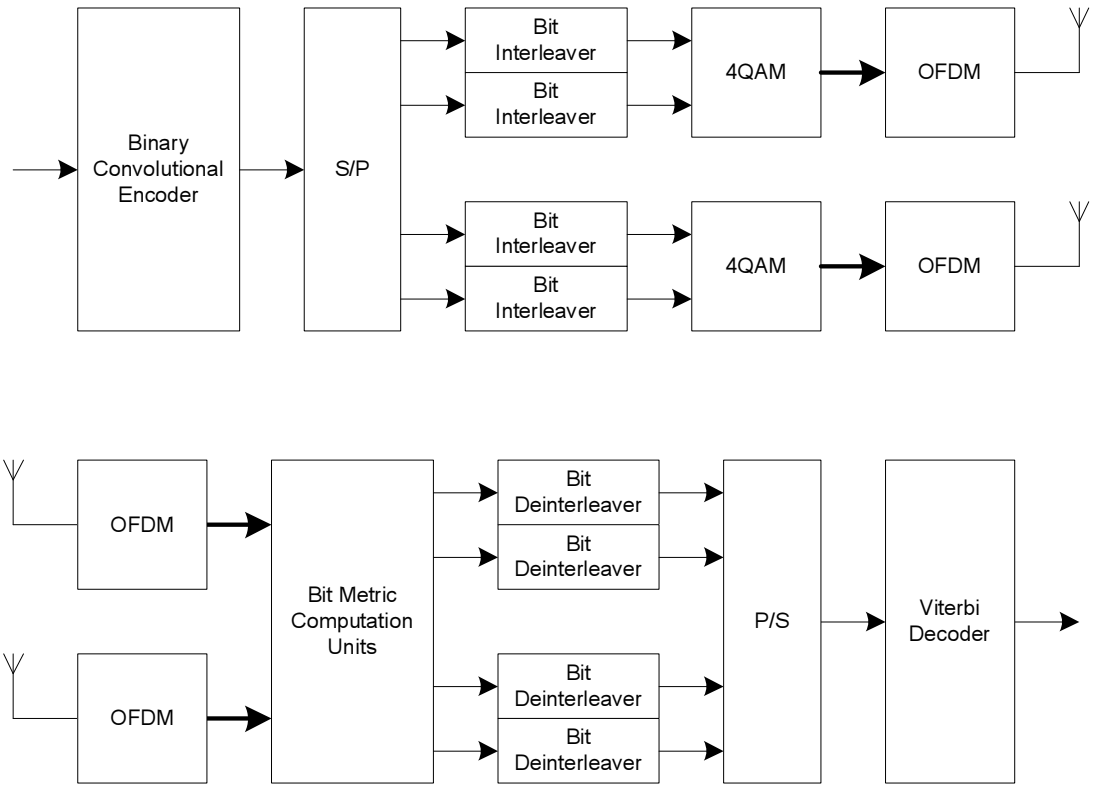

Figure 5.2: An example of transmitter and receiver in a 2×2 ST-BICM system with 4-QAM mapping

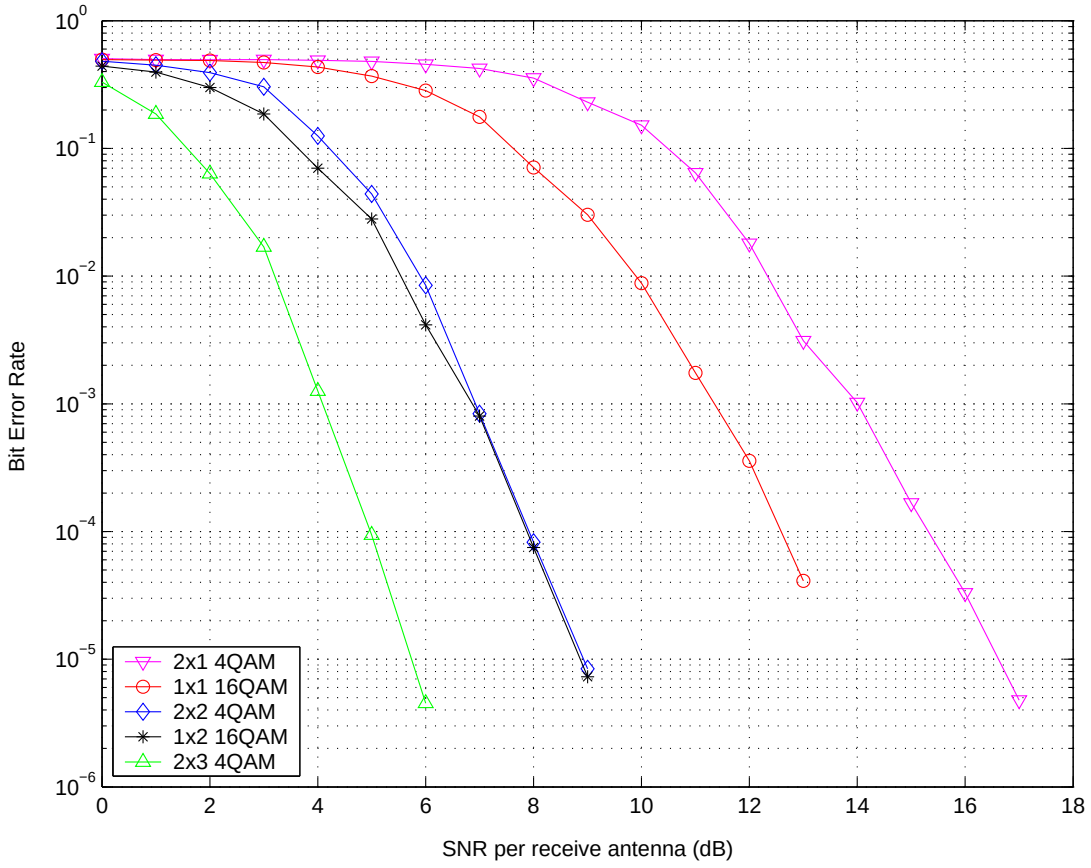

Figure 5.3: BER performance of ST-BICM for 4 b/s/Hz with various antenna configuration

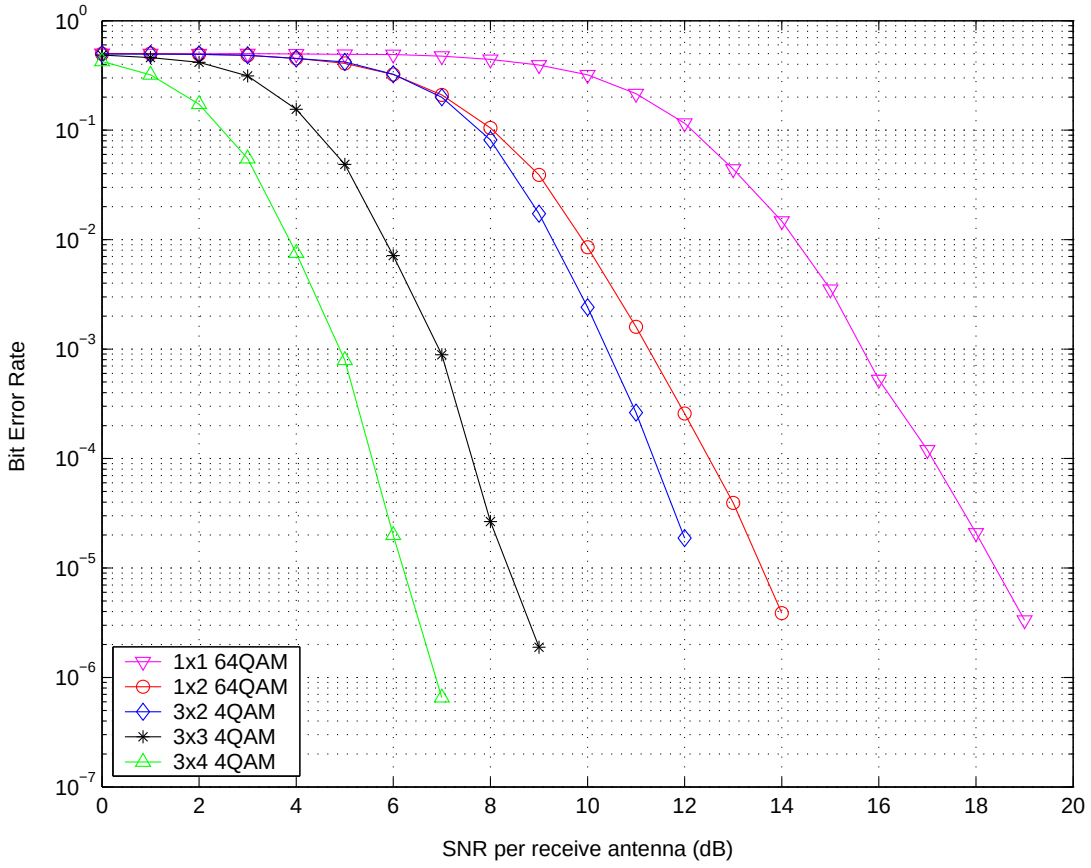

Figure 5.4: BER performance of ST-BICM for 6 b/s/Hz with various antenna configuration

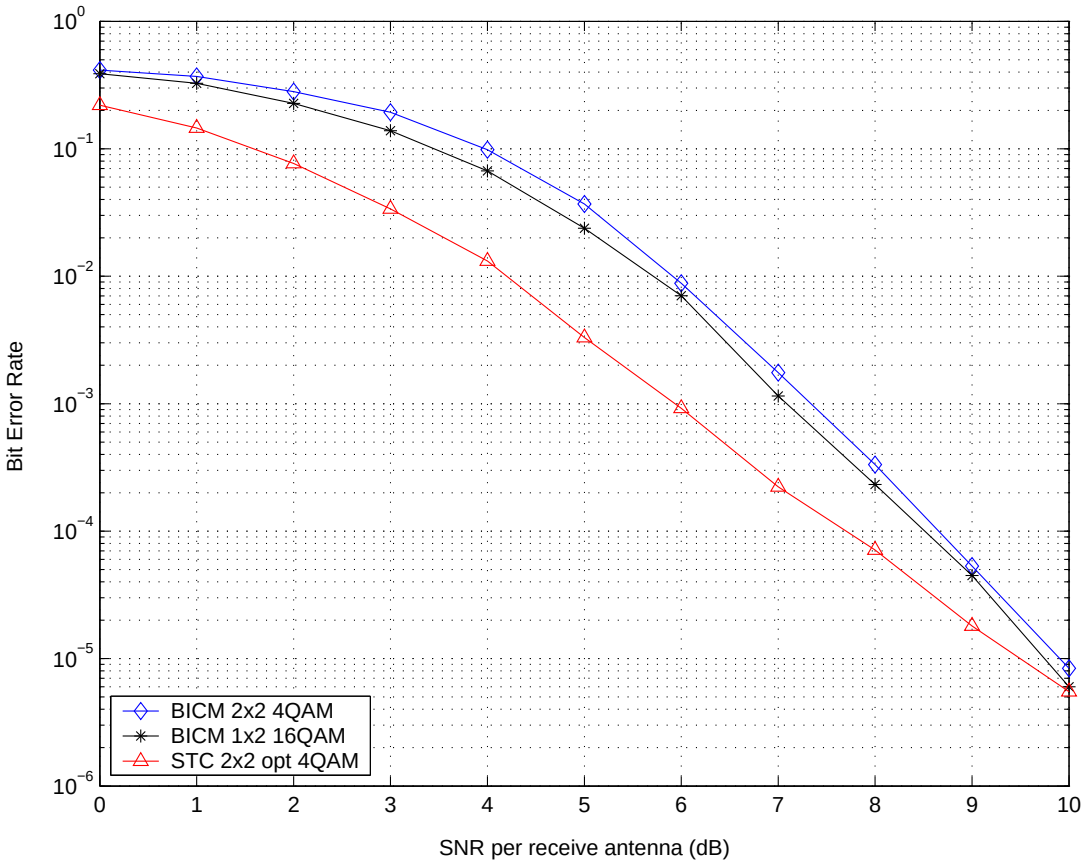

Figure 5.5: BER performance of STC and ST-BICM for 4 bit/sec/Hz

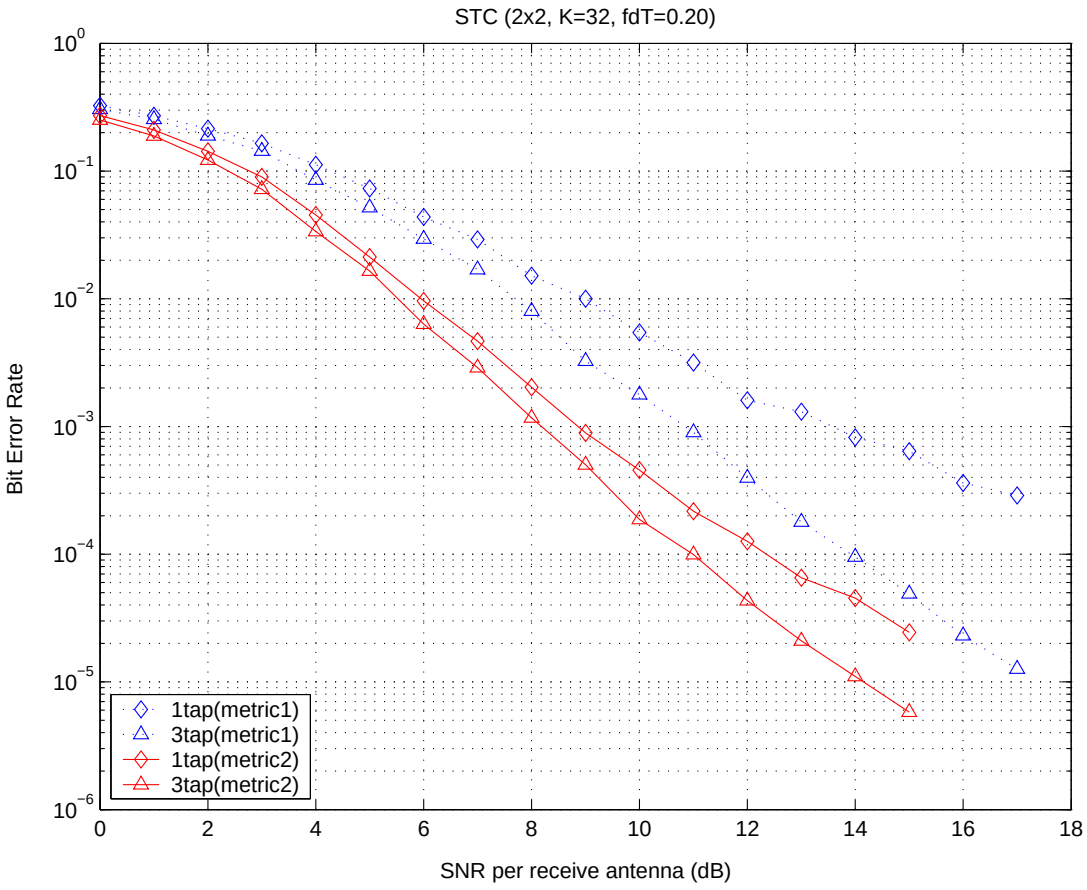

Figure 5.6: BER performance of STC with q-tap MMSE equalizer

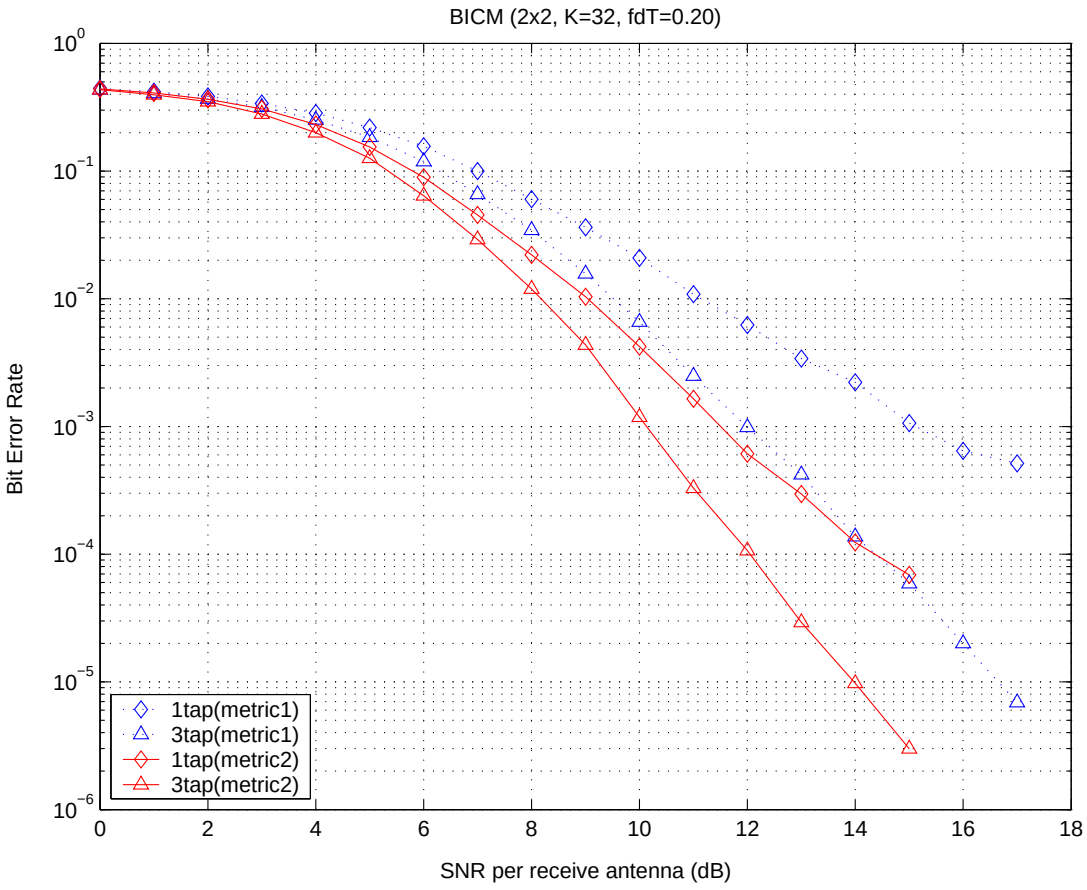

Figure 5.7: BER performance of ST-BICM with q-tap MMSE equalizer

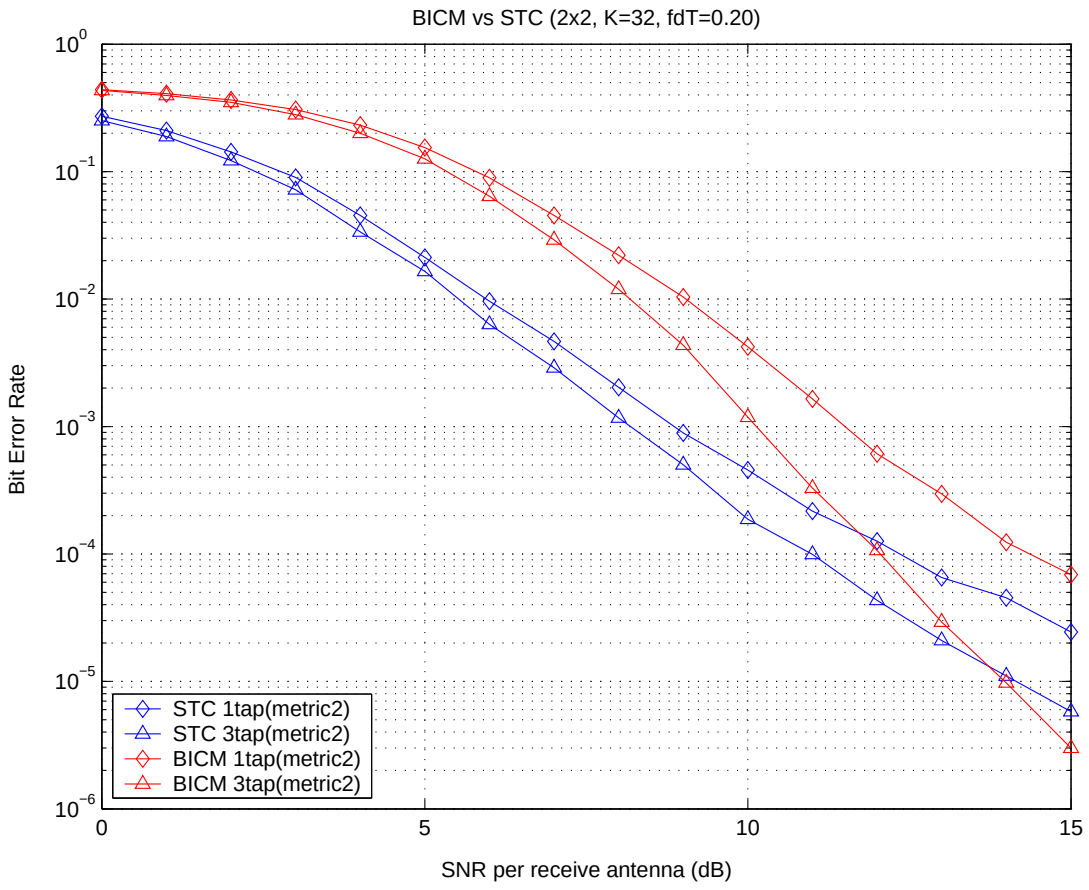

Figure 5.8: BER performance of STC and ST-BICM with q-tap MMSE equalizer

q	η from [12]	η from [1]	G^T
4	2	$\sqrt{8}$	$\begin{pmatrix} 2 & 0 & 1 & 2 \\ 2 & 2 & 2 & 1 \end{pmatrix}$
8	$\sqrt{12}$	4	$\begin{pmatrix} 0 & 2 & 1 & 0 & 2 \\ 2 & 1 & 0 & 2 & 2 \end{pmatrix}$
16	$\sqrt{12}$	$\sqrt{32}$	$\begin{pmatrix} 0 & 2 & 1 & 1 & 2 & 0 \\ 2 & 2 & 1 & 2 & 0 & 2 \end{pmatrix}$
32	$\sqrt{12}$	6	$\begin{pmatrix} 2 & 0 & 1 & 2 & 1 & 2 & 2 \\ 2 & 2 & 0 & 1 & 2 & 0 & 2 \end{pmatrix}$

Table 5.1: Optimum q-state 2 b/s/Hz 4-QAM STCs in [1]

CHAPTER 6

Conclusion

6.1 Dissertation Summary

Chapter 2,3 present a practical solution for designing a robust OFDM system in fast fading channels, using a q-tap MMSE equalizer with BICM. Chapter 4,5 suggest a practical method for designing robust MIMO-OFDM systems in fast fading channels, using a q-tap MMSE equalizer with either ST-BICM or STCs.

Chapter 2 began with the derivation of a mathematical model for OFDM systems in fast fading channels. An interchannel interference expression and its properties were presented. As a solution to reduce ICI, a frequency domain MMSE equalizer was suggested. It was shown that a conventional MMSE approach is not feasible, due to the large number subchannels of OFDM. Using the energy localization property of ICI, the complexity of the MMSE equalizer can be reduced significantly without much performance degradation.

Chapter 3 introduced BICM, which performs better than TCM in Rayleigh fading channels. The combination of q-MMSE equalizer and BICM was suggested in order to reduce ICI and achieve large coding gain under fast fading scenarios.

For the combination, several new bit metrics were suggested. Simulation results showed the robustness of the suggested schemes.

Chapter 4 extended the equalization method for SISO-OFDM systems to MIMO-OFDM systems. A new MIMO-OFDM model was derived by extending the system model described in Chapter 2. As a solution for both combating ICI and processing mixed signals from several transmit antennas, a q-tap MMSE equalizer was suggested. Simulation results showed the q-tap MMSE equalizer works well under various scenarios.

Chapter 5 compared STCs and ST-BICM. Decoding methods for STCs and ST-BICM systems under quasi-static Rayleigh channels were derived. ST-BICM offers large flexibility in terms of the number of antenna, the size of signal constellation, and code rate, whereas STCs are required to be redesigned for optimization. Overall performance of the STCs is superior to the ST-BICM, but the performance difference become smaller as SNR increases. As an extension of Chapter 3, new metrics for both STCs and ST-BICM systems were developed, in order to combine the channel coding with the q-tap MMSE equalizer designed in Chapter 4. Simulation results showed that, for both STCs and ST-BICM, new suggested metrics and 3-tap MMSE equalizers provide 2-3 dB gains at a 10^{-5} bit error rate.

6.2 Future Work

In this thesis it is assumed that the channel state information (CSI) is known to the receiver. One direction for the future work is to develop channel estimation algorithms applicable to fast fading channels. Conventional channel estimation algorithms do not fit into this work, since most algorithms assume the channel is quasi-static during an OFDM symbol period. To achieve best results from the MMSE equalizers and the channel coding, channel estimation cannot be neglected.

Even though the combination of the equalizers and codes show very robust performance in fast fading channels, it is not the best solution for all fast fading scenarios. Not only the trade-off of parameters for the equalizers and codes, but also adapting the system parameters, such as the number of OFDM tones N, is important. For example, when the channel is more time-selective than frequency-selective, it is good idea to use single carrier systems instead of OFDM, in order to avoid severe ICI impairments It would be interesting to see how to formally characterize the system design in a given wireless channel condition.

References

[1] R. S. Blum, "Some analytical tools for the design of space-time convolutional codes," *IEEE Trans. Commun.*, vol. 50, no. 10, pp. 1593–1599, Oct. 2002.

[2] R. W. Chang, "Synthesis of band-limited orthogonal signals for multichannel data transmission," *Bell Syst. Tech. J.*, vol. 45, pp. 1775–1796, Dec. 1966.

[3] B. R. Saltzberg, "Performance of an efficient parallel data transmission system," *IEEE Trans. Commun.*, vol. COM-15, pp. 805–811, Dec. 1967.

[4] R. W. Chang and R. A. Gibby, "A theoretical study of performance of an orthogonal multiplexing data transmission scheme," *IEEE Trans. Commun.*, vol. COM-16, pp. 529–540, Aug. 1968.

[5] L. J. Cimini, "Analysis and simulation of a digital mobile channel using orthogonal frequency division multiplexing," *IEEE Trans. Commun.*, vol. COM-33, pp. 665–675, July 1985.

[6] W. G. Jeon, K. H. Chang, and Y. S. Cho, "An equalization technique for orthogonal frequency-division multiplexing systems in time-variant multipath channels," *IEEE Trans. Commun.*, vol. 47, no. 1, pp. 27–32, Jan. 1999.

[7] Z. Wang and G. B. Giannakis, "Wireless multicarrier communications," *IEEE Signal Processing Mag.*, pp. 29–48, May 2000.

[8] Y. S. Choi, P. J. Voltz, and F. A. Cassara, "On channel estimation and detection for multicarrier signals in fast and selective rayleigh fading channels," *IEEE Trans. Commun.*, vol. 49, no. 8, pp. 1375–1387, Aug. 2001.

[9] G. Ungerboeck, "Channel coding with multilevelphase signals," *IEEE Trans. Inform. Theory*, vol. IT 28, pp. 55–67, Jan. 1982.

[10] E. Zehavi, "8-psk trellis codes for a rayleigh channel," *IEEE Trans. Commun.*, vol. 40, no. 5, pp. 873–884, May 1992.

[11] G. J. Foschini, "Layered space-time architecture for wireless communication in a fading environment when using multi-element antennas," *Bell Labs Tech. J.*, pp. 41–59, Aug. 1996.

[12] V. Tarokh, N. Seshadri, and A. R. Calderbank, "Space-time codes for high data rate wireless communications: Performance analysis and code construction," *IEEE Trans. Commun.*, vol. 46, pp. 357–366, Mar. 1998.

[13] S. L. Ariyavisitakul, "Turbo space-time processing to improve wireless channel capacity," *IEEE Trans. Commun.*, pp. 1347–1359, Aug. 2000.

[14] S. Alamouti, "A simple transmit diversity technique for wireless communications," *IEEE J. Select. Areas Commun.*, vol. 16, no. 9, pp. 1451–1458, Oct. 1998.

[15] P. W. Wolniansky, G. J. Foshini, G. D. Golden, and R. A. Valenzuela, "V-BLAST: An architecture for realizing very high data rates over the righ-scattering wireless channel," in *Proc. Int. Symp. Signals, Syst., Electron*, 1998, pp. 295–300.

[16] G. J. Foschini and M. J. Gans, "On limits of wireless communications in a fading environment when using multiple antennas," *Wirelss Pers. Commun.*, vol. 6, pp. 311–335, 1998.

[17] S. Müller-Weinfurtner, "Coding approaches for multiple antenna transmission in fast fading and OFDM," *IEEE Trans. Wireless Commun.*, vol. 1, no. 4, pp. 563–571, Oct. 2002.

[18] A. F. Naguib, N. S. V. Tarokh, and A. R. Calderbank, "A space-time coding modem for high-data-rate wireless communications," *IEEE J. Select. Areas Commun.*, vol. 16, pp. 1459–1478, Aug. 1998.

[19] V. Tarokh, A. F. Naguib, N. Seshadri, and A. R. Calderbank, "Space-time codes for high data rate wireless communication: Performance criteria in the presence of channel estimation errors, mobility and multiple paths," *IEEE Trans. Commun.*, vol. 47, pp. 199–207, Feb. 1999.

[20] S. B. Weinstein and P. M. Ebert, "Data transmission by frequency-division multiplexing using the discrete fourier transform," *IEEE Trans. Commun.*, vol. COM-19, pp. 628–634, 1971.

[21] J. A. C. Bingham, "Multicarrier modulation for data transmission: An idea whose time has come," *IEEE Commun. Mag.*, vol. 28, no. 5, pp. 5–14, 1990.

[22] H. Sari, G. Karam, and I. Jeanclaude, "Transmission techniques for digital terrestrial TV broadcasting," *IEEE Commun. Mag.*, vol. 33, no. 2, pp. 100–109, 1995.

[23] D. L. Goeckel, "Coded modulation with nonstandard signal sets for wireless OFDM systems," in *Proc. Conf. Inform. Sci. Syst.*, 1999, pp. 791–795.

[24] R. S. Blum, "New analytical tools for designing space-time convolutional codes," in *Proc. Conf. Inform. Sci. Syst.*, Princeton, NJ, 2000, pp. WP3.1–WP3.6.

[25] R. S. Blum, Y. G. Li, J. H. Winters, and Q. Yan, "Improved space-time coding for MIMO-OFDM wireless communications," *IEEE Trans. Commun.*, vol. 49, no. 11, pp. 1873–1878, Nov. 2001.

[26] W. Firmanto, B. S. Vucetic, and J. Yuan, "Space-Time TCM with improved performance on fast fading channels," *IEEE Commun. Lett.*, vol. 5, pp. 154–156, Apr. 2001.

[27] S. A. Zummo and S. A. Al-Semari, "Space-Time coded QPSK for rapid fading channels," in *Proc. Int. Symp. Pers., Indoor Mobile Radio Commun.*, London, U.K., 2000, pp. 504–508.

[28] ——, "A decoding algorithm for I-Q space-time coded systems in fading environments," in *Proc. IEEE Veh. Technol. Conf.*, Boston, MA, 2000, pp. 331–335.

[29] A. Chindapol and J. A. Ritcey, "Bit-Interleaved coded modulation with signal space diversity in rayleigh fading," in *Conf. Rec. 33rd Asilomar Conf. Signals, Syst., Comput.*, 1999, pp. 1003–1007.

[30] G. Raleigh and J. M. Cioffi, "Spatio-temporal coding for wireless communication," *IEEE Trans. Inform. Theory*, vol. 44, pp. 744–765, Mar. 1998.

[31] A. F. Naguib, V. Tarokh, N. Seshadri, and A. R. Calderbank, "A space-time coding modem for high-data-rate wireless communications," *IEEE J. Select. Areas Commun.*, vol. 16, pp. 1459–1478, Oct. 1998.

[32] V. Tarokh, H. Jafarkhani, and A. R. Calderbank, "Space-time block coding for wireless communications: Performance results," *IEEE J. Select. Areas Commun.*, vol. 17, pp. 451–460, Mar. 1999.

[33] J. C. Guey, M. P. Fitz, M. R. Bell, and W. Y. Kuo, "Signal designe for transmitter diversity wireless communication systems over rayleigh fading channels," *IEEE Trans. Commun.*, vol. 47, pp. 527–537, Apr. 1999.

[34] V. Tarokh, H. Jafarkhani, and A. R. Calderbank, "Space-time block codes from orthogonal designs," *IEEE Trans. Inform. Theory*, vol. 45, pp. 1456–1467, July 1999.

[35] S. Baro, G. Bauch, and A. Hansmann, "Improved codes for space-time trellis coded modulation," *IEEE Commun. Lett.*, vol. 4, pp. 20–22, Jan. 2000.

[36] Q. Yan and R. S. Blum, "Improved space-time convolutional codes for quasi-static slow fading channels," *IEEE Trans. Signal Processing*, vol. 50, no. 10, pp. 2442–2450, Oct. 2002.

[37] J. Grimm, M. P. Fitz, and J. V. Krogmeier, "Further results in space-time coding for Rayleigh fading," in *Proc. 1998 Allerton Conf.*, 1998, pp. 391–400.

[38] J. Grimm, "Transmitter diversity code design for achieving full diversity on Rayleigh channels," Ph.D. dissertation, Purdue Univ., W. Lafayette, IN, 1998.

[39] I. Telatar, "Capacity of multi-antenna Gaussian channels," *Euro. Trans. Telecommun.*, pp. 585–595, Nov. 1999.

[40] G. Caire, G. Taricco, and E. Biglieri, "Bit-interleaved coded modulation," *IEEE Trans. Inform. Theory*, vol. 44, no. 3, pp. 927–946, May 1998.

[41] E. Biglieri, G. Taricco, and E. Viterbo, "Bit-Interleaved time-space codes for fading channels," in *Proc. Conf. Inform. Sci. Syst.*, Princeton, NJ, 2000, pp. WA4.1–WA4.6.

[42] G. Caire, G. Taricco, and E. Biglieri, "Recent results on coding for multiple-antenna transmission systems," in *Proc. 6th Int. Symp. Spread-Spectrum Tech. Appl.*, 2000, pp. 117–121.